Electrical and gas networks coupling through hydrogen blending under increasing distributed photovoltaic generation

Coupling Electricity and Gas Distribution with Hydrogen Blending: Infrastructure Modelling under Increasing Photovoltaic Generation

Marco Cavana, Andrea Mazza, Gianfranco Chicco, Pierluigi Leone*
Department of Energy "Galileo Ferraris", Politecnico di Torino
Corso Duca degli Abruzzi 24, 10129 Torino, Italy

*Corresponding author: Pierluigi Leone (pierluigi.leone@polito.it).

Abstract

Innovative interlinks between the electricity and the gas infrastructures have the twofold effect of solving production-consumption mismatches and decarbonizing the natural gas system by means of power-to-gas technologies producing hydrogen to be injected within the gas network. However, little is known on how this may impact the gas network operation.

This paper presents a methodology for modelling the interactions between electricity and gas distribution networks through the implementation of their physical models. A scenario of increasing penetration of distributed photovoltaic production is considered on a sample urban area built for the purpose of showing the potentiality of the methodology developed. Whenever the photovoltaic production exceeds the urban area consumption, the centralized production of hydrogen from power-to-gas and its injection into the gas network are considered. A total number of 24 injection scenarios were examined and compared to evaluate their impacts on fluid-dynamics and quality of the gas blends.

The results show a significant impact of the hydrogen injection, especially during the summer operations and when the injection rate is directly coupled with the hydrogen production, giving the first hints on the management of a multi-gas system in the context of integrated energy infrastructure at local level.

Keywords

renewable gas; gas network; power-to-gas; hydrogen blending; electricity distribution.

Highlights

- Surplus solar hydrogen injection strongly affects natural gas quality.
- Gas network fluid dynamics negligibly affected by hydrogen injection..
- Buffer required between hydrogen production and injection to maintain gas quality.
- Injection node choice affect the hydrogen receiving potential.

Acknowledgements

This work is part of the project “Heat in the Pipe” – bando “Metti in Rete la tua Ricerca” financed by Compagnia di San Paolo and Politecnico di Torino.

1 Introduction

With the European Directive 2018/2001/EC [1], the European Union (EU) updated its efforts on energy transition towards a more sustainable energy system for the decade 2020-2030,aiming to supply at least 32% of the EU's gross final consumption by renewables, in line with the Paris Agreement commitment.

Most scenarios agree that the general Renewable Energy Source (RES) goal of around 30% corresponds to a share of renewables on the electricity sector equal to 50%, thus implying significant impacts on the electrical system.

The deployment of Variable Renewable Energy Sources (VRES) such as photovoltaic and wind has already changed the traditional electrical system paradigm, both in terms of the management of geographically distributed and smaller size VRES plants, and in terms of solving production-consumption mismatches.

In the context of Distributed Energy Resources (DERs), small size photovoltaic (PV) systems have taken the lead during the past decade thanks to effective feed-in tariffs schemes [2]. However, their connection at medium or low voltage distribution networks have introduced a number of operational issues [3] including voltage problems [4], reverse power flows [5] as well as the need of storage systems [6]. In view of the further planned energy transition, these mentioned issues will be more and more critical, asking for additional flexibility. Flexibility within the power system may come from different sources such as the presence of a suitable fleet of back-up power plants, the setting up of Demand-Response strategies, enhanced grid interconnection, and energy storage solutions [7]. Which solution will have the prominent role is difficult to determine at the moment. For instance, in [8] it is reported that grid expansion may be the most cost effective solution in order to enhance the flexibility of the electric system. Nonetheless, in case of a fast increase of E-RES within the energy system, then the implementation of storage systems may be more effective. This has to deal with the timings related to the planning and the actual renovation rate of an infrastructural asset.

Concerning storage technologies, besides traditional and well established options such as pumped hydro, batteries have known increased interest among researcher and stakeholders, with several pilots and the first grid scale installations [9]. Power-to-gas (P2G) technologies have been gaining increased interest lately as an unconventional storage pathway. In fact, they entail the production of a fuel gas (hydrogen or synthetic methane) using surplus energy from renewables as energy input, thus fixing the energy excess within chemical bonds, producing a commodity or an energy vector that is alternative and more easily storable than electricity.

Particularly, hydrogen has been getting renovated attention in the last years as key enabler for the energy transition [10]. As an energy vector, crucial is the opportunity that hydrogen offers to avoid the requirements for instantaneous supply-demand balancing. According to [11], hydrogen can play a major role in decarbonizing the energy system thanks to its versatility of use in transportation, electricity and heating provision, storage and grid services and as a commodity for industrial applications.

Even though most of the hydrogen applications have reached the commercial stage only in some sectors, and their uptake within the future energy system is considered to happen no earlier than a few decades according to international [12] and national [13] scenarios, hydrogen is gaining a serious industrial interest among natural gas sector stakeholders (e.g. British [14], Italian [15] and Dutch [16] gas network operator). Today's gas network plays a unique role for the distributed delivery of heat for domestic and industrial use. Its substitution may not be as easy as it seems [17]. As the peak demand for heat is about five times greater than electricity one [18] a full electrification of the heating sector would require reinforcement of the whole power infrastructure, requiring very high costs on the final consumers [19]. The natural gas sector finds itself in a controversial position, being considered as one of the key enablers of the energy transition in the short run, but with several scenarios that foresee a necessary phasing out to meet long-term goals of deep decarbonisation. This contradictory trend may have a serious implication in the economical sustainability of the transition, generating the so-called "carbon lock-in" situation [20], caused by the its infrastructural nature [21].The future development of existing energy network infrastructures has a fundamental role in the definition of the roadmaps for energy transition, resulting in a complex co-evolutionary process. In this sense, the European Networks of Transmission System Operators for Electricity and Gas (ENTSO-E and ENTSOG) have recently started an integrated planning exercise of the energy infrastructures aiming towards the power and gas sector coupling. For the first time in 2018, the Ten Year Network Development Plan 2018 (TYNDP-2018) [22] was built on energy scenarios jointly agreed, showing an actual interest in building the so called "hybrid energy infrastructure" through a fully sector coupling. A very similar commitment is emerging at the distribution system level, as it is clearly stated in [23] and [24].

The practice of hydrogen production through power-to-gas or steam reforming with CCS and its subsequent blending within the already existent gas infrastructure is an example of electricity-gas sector coupling [25] and it is considered an innovative and effective decarbonisation option [26]. In fact, natural gas-hydrogen blends

(sometimes referred as H_2NG) contribute to lower the carbon footprint of the whole gas sector value-chain ("greening of the gas network" [27]). It is framed within the broader context of *renewable gas* injection (i.e. bio-methane [28], synthetic natural gas [29], hydrogen…), a practice that, by 2050, appears to be more economically convenient than 100% electrification according to recent studies, with annual savings ranging between 94 [30] and 138 [31] billion € per year at European level.

On a more technical basis, the white paper published by the Sustainable Gas Institute (2017) [32] presents a comprehensive study on the various options for a greener gas network. Focusing on the hydrogen case, a number of technical aspects should be addressed because of the considerably different properties that hydrogen has with respect to natural gas. An extensive review of the opportunities and the criticalities of hydrogen admixture within the current gas infrastructure is given in [33]. As of pipeline integrity, the main concern is related to steel embrittlement: an increasing concentration of hydrogen within the bulk of metal causes a decrease of the yield stress value [34]. The hydrogen-to-metal permeation mechanism have been mainly studied in case of metal exposure to 100% hydrogen [35] and in [36], the fast transient behaviour of the same pipeline modelled with 100% natural gas and 100% hydrogen have been compared to highlight how critical the switch to hydrogen may be. More promising results have been obtained by the extensive experimental campaign presented in [37] where both polymers and steel pipes already used in the Danish distribution and transmission system have been exposed to hydrogen for 4 years without showing detrimental effects. Not only the material compatibility but also the transmission capacity has to be taken into account: in [38] an optimization model for the repurposing of the high pressure transmission infrastructure is presented showing the possible need to substitute pipelines and add compression capacity.

In [39] maximum values of admissible hydrogen concentrations are given for a number of different areas of the overall gas system. No major issues should be met up to concentration of 15%, even though in presence of Compressed Natural Gas (CNG) fuelling station or gas turbines the limit may need to be 1% or lower.

Concerning users' appliances, the ones commercialised in Europe since the '90s under the Gas Appliances Directive (Gas Appliances Regulation as for 2019 [40]) should be able to withstand hydrogen molar fraction up to 23% according to the testing procedures they have to undergo (according to [41]). However, burning hydrogen-enriched methane have an impact on domestic boilers [42] and on industrial burners [43], requiring adjusting measures in order to limit negative impact on efficiency and pollutant emission, even for hydrogen

blends lower than 10% . An extensive analysis of gas interchangeability has been conducted in [44] for domestic appliances stating that the natural gas composition has also a role in determining hydrogen acceptability.

Hydrogen blending has thus a very different and non-negligible impact on the various levels of the gas sector, and all the literature and the stakeholders agree on the need to pursue additional research. This reflects also at the regulatory level, with attempts towards harmonization of the national natural gas quality requirements at the European level (M/400 EN [45]). The latest achievement of the European Committee for Standardization (CEN) is the publication of the norm EN 16726:2019 [46] on standardisation of gas quality (group H). Here the case of hydrogen injection is mentioned in an informative annex, reporting the results already presented in [39] and concluding with the impossibility of setting a common limiting value for hydrogen in the European infrastructure and recommending a case by case analysis.

These uncertainties and barriers justify the interest towards the incorporation of hydrogen blending in the modelling of the energy networks. This paper considers the integration between the medium voltage (MV) electricity grid and the medium pressure gas network through power-to-hydrogen solutions. Electricity and gas networks are jointly tested under 24 test cases with different renewable penetration levels and hydrogen injection scenarios. The simulation algorithms solve the power flow equations for the electrical network under increasing levels of distributed photovoltaic production, and the energy balance in the gas network under different injection cases of (growing) hydrogen availability. Cases with no injection limits are analysed to clarify the impact of the blending practice under growing local RES penetration. Different injection scenarios are considered and compared in order to carry out an overall assessment of the possible options.

The specific contributions of this paper are:

1. The implementation of a simulation tool for the integration between electricity and gas networks, able to deal with different cases, ranging from fully decoupled networks to combined infrastructures.

2. The assessment of the benefits of coupling electricity and gas networks to increase the possibility to avoid reverse power flows and branch overloading in the electrical network, for different RES penetrations.

3. The analysis of the impact of hydrogen injection practices on the fluid-dynamics of the gas network and on the natural gas quality.

The next sections of this paper are organised as follows. Section 2 illustrates the modelling tools for electricity and gas networks, as well as the methodology set up for the networks integration through power-to-gas. Section 3 is devoted to the description of the sample urban context under the electrical network and the gas system point of view. Section 4 presents the results of the several test cases, which are finally discussed in Section 5. The last section contains the conclusions.

2 Combined simulation of Electricity and Gas Network Infrastructures

2.1 State of the art of electricity and gas network simulation with hydrogen blending

The subject of a fully integrated energy system in which the different network infrastructures exchange energy flows is gaining interest in the literature. Many of the power and gas integrated simulation frameworks have originated form the optimization problem of the entire energy system under higher V-RES such as in [47]. In [48], the authors presents a co-simulation platform of both power and gas transmission system aiming to evaluate the gas turbine ramping effects on the gas system. The gas system is modeled using the dynamic gas network solver presented in [49], while the power network is modeled by means of a different dedicated tool [50]. In [51] a methodology for the modelling of the gas network as an electrical analogy is given in order to ease the creation of co-simulation frameworks. A similar approach is adopted in [52], where a unified energy flow formulation is developed to simulate scenarios of bi-directional energy exchange between gas and power sector by means of Power-to-Methane. The Power-to-Hydrogen pathway is instead addressed in [53], [54] and [55]. In [54] and [55] optimal power flow for a national power transmission system is solved considering the possibility to use P2G as an effective option to store otherwise the curtailed renewable energy. Subsequently, the impact of hydrogen injection on the transmission pipeline system is evaluated with different admissible hydrogen concentration limits. In [56], an economic dispatch of a multi-energy system is performed under distributed injection scenarios and addressing a low pressure natural gas grid. The thermal need may be met by either natural gas or electricity depending on the costs of the commodity. These integrated simulation platforms, however, do not provide a detailed model of the fluid-dynamic of the gas network under non-conventional gas injections and do not consider any gas quality transport time along the pipelines. More detailed gas network model are adopted in the following references. In [57] the fluid-dynamic of a transmission pipeline trunk with an hydrogen injection points is modelled, assuming that the amount of injected hydrogen

is such that the hydrogen molar fraction would not be exceeding the 5% limit. In [58], a detailed modelling framework for gas quality perturbation along a high pressure, single-pipeline system is presented. An example of hydrogen blending modelling within a real regional gas transmission network is given in [27], where the maximum admissible hydrogen injection is calculated in order for the H_2-NG admixture to be compliant with the technical regulations and the storable electrical energy determined (for each node of the network). Similarly, in [59] the study is performed on a real municipal gas network. The latter two works focus specifically on the gas network modelling using a proper equation of state that is sensitive to the varying gas composition [60]. Another example of gas network modelling with distributed source of unconventional gases is given in [61] where a simpler physics regarding gas quality is adopted.

The modelling of sectorial coupling between power and gas sector has thus been widely addressed at the transmission system level, while investigations are lacking for distribution systems, with district or urban energy infrastructures characterized by lower voltage and pressure level. In the framework of increasing the spreading of distributed RES, the sector coupling may offer innovative solutions for energy surplus management and decarbonisation of the gas system.

2.2 Proposed methodology

A dedicated simulation framework has been set up to study the interactions between electricity and gas networks. The simulator is made of two different models, one for the power flow calculation within the electricity grid, and the other one for the gas flow assessment in the pipeline network. The mathematical features of both models are illustrated below. The two models need to be linked by means of a specific routine in order to mimic the interrelations between the two networks. This routine may change with respect to the level of integration between the two sectors, ranging from the fully decoupled case to proper combined simulation of the infrastructures. For the application shown in this paper, the electrical and gas networks are assumed in steady-state conditions, thus addressing the time-dependent simulation as a sequence of steady states at a time step consistent with the availability of metered data to construct the electrical load time series.

2.3 Common features of network representation

The electrical and gas networks considered are at the distribution level, that is, they are no directly connected to the final users, with the exception of industrial ones. Therefore, the nodes of these networks are

generally not the same. The structure of both networks are radial in this case and are represented as oriented graphs, in which the branches are the lines (for the electrical network) and the pipelines (for the gas network) and the nodes are the junctions between two or more lines or pipelines. Furthermore, for each radial network, the branches are numbered in a unique way with the number of their outlet node. By considering *N* nodes and *M* branches, the information about the connections is fully stored in the *branch-to-node incidence matrix* $\boldsymbol{X} = \{x_{j,i}\} \in \mathcal{N}^{M,N}$, generally defined as follows:

$$x_{j,i} = \begin{cases} +1 & \text{if node } i \text{ is the inlet node of branch } j \\ -1 & \text{if node } i \text{ is the outlet node of branch } j \\ 0 & \text{otherwise} \end{cases} \quad (1)$$

For the specific application to an electrical network with N_E nodes and M_E branches and to a gas network with N_G nodes and M_G branches, the corresponding branch-to-node incidence matrices are identified as $\boldsymbol{X}_\mathrm{E} \in \mathcal{N}^{M_\mathrm{E},N_\mathrm{E}}$ and $\boldsymbol{X}_\mathrm{G} \in \mathcal{N}^{M_\mathrm{G},N_\mathrm{G}}$, respectively.

2.4 Electrical Network Model

The solution of an electrical network consists, per every time step of the horizon considered, in the determination of the voltages $\mathbf{v} = \left[\bar{V}_1 \ , \dots , \bar{V}_{N_\mathrm{E}}\right]^\mathrm{T}$ at each node and of the currents $\mathbf{i}_\mathrm{B} = \left[\bar{I}_1 \ , \dots , \bar{I}_{M_E}\right]^\mathrm{T}$ flowing in each branch. When the loads at the nodes are represented with the constant power model (as most frequently happens), the equation linking the nodal currents (also called shunt currents $\mathbf{i}_\mathrm{S} = \left[\bar{I}_1, \dots , \bar{I}_{M_\mathrm{E}}\right]^\mathrm{T}$) and the nodal voltages **v** is:

$$\bar{S}_i = P_i + jQ_i = \bar{V}_i \, \bar{I}_{S_i}^{*} \qquad \forall \, i^{th} \, node \quad (2)$$

where $\bar{S}_i$ is the complex power that is absorbed by each i^{th} node, P_i is the active power and Q_i is the reactive power. Equation (2) is non-linear, thus an iterative solution strategy is needed. The backward-forward sweep (BFS) method is here applied, being suitable for radial networks, as well as for weakly meshed networks [62]. The BFS owes its name to the structure of each iteration, which is composed of two computation steps. The first is called "backward sweep" and consists in the application of the Kirchhoff's current law by efficiently considering the inverse incidence matrix $\boldsymbol{\Gamma} = \boldsymbol{X}_\mathrm{E}^{-1}$, resulting in the following equation:

$$\mathbf{i}_\mathrm{B}^{(k)} = \boldsymbol{\Gamma}^\mathrm{T} \, \mathbf{i}_\mathrm{S}^{(k-1)} \quad (3)$$

in which the entries $\bar{I}_{\mathrm{S}i}^{(k)}$ of the node currents vector $\mathbf{i}_{\mathrm{S}}^{(k)}$ (with currents exiting from the nodes) are determined starting from the nodal equations and considering the node voltages $\bar{V}_i^{(k-1)}$ determined at the previous iteration (with an initial value for the nodal voltages $\bar{V}_i^{(0)}$ at the first iteration, e.g., set to the slack node voltage V_0 or to the "flat profile" with voltages equal to 1 per unit for all the nodes excluding the slack node):

$$\bar{I}_{\mathrm{S}i}^{(k-1)} = \left(\frac{\bar{S}_i}{\bar{V}_i^{(k-1)}} \right)^* \qquad \forall\, i^{th}\ node \tag{4}$$

Once the line currents vector at the *k*-th iteration $\mathbf{i}_{\mathrm{B}}^{(k)}$ is determined, the "forward sweep" is executed by using the line equation in its matrix form. Starting from the slack node voltage V_0 (with null reference angle) and from the unity vector $\mathbf{1} \in \mathcal{N}^{N_{\mathrm{E}},1}$, the node voltage vector at the iteration k $\mathbf{v}^{(k)}$ is updated as:

$$\mathbf{v}^{(k)} = V_0\, \mathbf{1} - \mathbf{\Gamma}\ \ \mathbf{Z_B}\, \mathbf{i}_{\mathrm{B}}^{(k)} = V_0\, \mathbf{1} - \mathbf{\Gamma}\ \ \mathbf{Z_B}\, \mathbf{\Gamma}^{\mathrm{T}}\, \mathbf{i}_{\mathrm{S}}^{(k-1)} \tag{5}$$

in which the series impedances of the branches are included in the diagonal matrix $\mathbf{Z_B} = \mathrm{diag}\left(\bar{Z}_1\ , \ldots, \bar{Z}_{M_E}\right)$.

The stop criterion for the BFS method depends on the user-defined tolerance ε. At iteration k, the iterative process stops if the following condition is satisfied:

$$\max_{i=1,..N_{\mathrm{E}}} \left\{ \frac{\left| \bar{V}_i^{(k)} - \bar{V}_i^{(k-1)} \right|}{\bar{V}_i^{(k)}} \right\} < \varepsilon \tag{6}$$

2.5 Gas Network Model

The fluid-dynamic model of the gas network infrastructure presented in [27] and validated in [63] has the capability to treat natural gas as a mixture of light hydrocarbons and other typical compounds. The composition of the modelled gas flow may vary along the network in case of a distributed injection of unconventional gases (e.g., hydrogen). This feature makes the model perfectly fitting the purpose of this work, thus it has been adapted to enable simulations at different time steps and to incorporate the interaction with the electrical distribution network in a given number of nodes.

The solution of a gas network consists of the determination of the pressure $\mathbf{p} = \left[p_1, \ldots, p_{N_G}\right]^{\mathrm{T}}$ at each nodes and of the mass flow rate $\mathbf{g} = \left[G^{(1)}, \ldots, G^{(M_G)}\right]^{\mathrm{T}}$ through each branch. In case of studies involving the injection of unconventional gases within the network infrastructure (such as hydrogen blending), the gas composition

$\mathbf{c}_i = [c_{1,i}, \dots, c_{\kappa,i}]$ needs to be determined for each i^{th} node. The vector $\mathbf{c}_i$ contains the composition of all the κ of chemical species referred to the node *i*. All the nodal loads are expressed in terms of thermal needs $\boldsymbol{\varphi}_{\text{ext}} = [\Phi_1, \dots, \Phi_{N_G}]$, which needs to be converted to mass flow rates exchanged with the external environment $\mathbf{g}_{\text{ext}} = \{G_{ext_i}\} \in \mathcal{R}^{N_G,1}$ by means of the following equation:

$$G_{ext_i} = \frac{\Phi_i}{HHV_i} \qquad \forall\, i^{th}\ node \tag{7}$$

where HHV_i is the higher heating value of the gas at node *i*, which is determined by the natural gas composition. The following sign rule is assumed:

$$G_{ext_i}: \begin{cases} > 0\,, if\ node\ i^{th}\ is\ \ a\ consumption\ node \\ < 0, if\ node\ i^{th}\ is\ an\ injection\ node \\ = \ 0, if\ no\ mass\ flow\ is\ exchanged\ with\ the\ external\ environment\ at\ node\ i^{th} \end{cases} \tag{8}$$

Given that the gas composition is one of the output variables, a tentative value needs to be assumed at the beginning of each time iteration. Once a tentative value of $\mathbf{g}_{\text{ext}}$ is obtained, the fluid-dynamic problem may be tackled. It is solved through the coupled solution of continuity and momentum equations:

Continuity equation: $$\boldsymbol{X}_{\text{G}}^{\text{T}}\,\mathbf{g} + \mathbf{g}_{\text{ext}} = \mathbf{0} \tag{9}$$

Momentum equation: $$\mathbf{g} = \boldsymbol{Y}\,\Delta\mathbf{p} \tag{10}$$

where:

$$\Delta\mathbf{p} = \boldsymbol{X}_{\text{G}}\ \mathbf{p} \tag{11}$$

Equation (10) is the linearized version of the momentum equation, resulting from the application of the electrical analogy, which is based on the definition of the pseudo-conductance of a pipe as follows:

$$Y_j(p) = A\frac{(p_{in}+p_{out})^{0,5}}{|p_{in}-p_{out}|^{0,5}}\left[\frac{D}{Z_{av}RT_{av}f_{av}L}\right]^{0,5} \quad \forall\, j^{th}\ pipe \tag{12}$$

where p is the fluid pressure [Pa], T is the temperature of the fluid [K], R is the specific gas constant [J/(kg · K)], Z is the compressibility factor [-], A is the pipeline cross section [m^2], D is the pipeline diameter [m], and f is the dimensionless friction factor calculated through the Colebrook-White equation [64]. The subscript *av* stands for averaged quantities along the pipe length, being pressure dependent.

As for the line impedance in the electric case, the further definition of the diagonal pseudo-conductance matrix $\boldsymbol{Y} \in \mathcal{R}^{M_G,M_G}$ is necessary to perform the operations in matrix form.

It is worth noting that it is a function of the pressure itself thus an iterative solution method is required.
The closure relation in order to be able to solve the coupled mass and momentum set of equation is given by the equation of state for real gases:

$$Z = \frac{p}{\rho RT} \tag{13}$$

where ρ is the fluid density [kg/m^3]. The compressibility factor $Z = Z(p, T, \mathbf{c})$ is defined through a pressure-dependent virial equation which is a function of pressure, temperature and gas composition vector $\mathbf{c}_i$. The virial coefficients are obtained through the application of the so-called mixing rule detailed in [65], in which the coefficients are specified by the s-GERG88 method – ISO standard [60].

For every time step *t*, knowing the energy needs of the users $\boldsymbol{\varphi}_{\text{ext}}(t)$, the pressure of the gas at injection points $p_{\text{set}}(t)$ and its composition $\boldsymbol{C}_{\text{ent}}(t) = \{\mathbf{c}_{\text{ent}}(t)\} \in \mathcal{R}^{N_{\text{G}},\kappa}$, the fluid dynamic problem represented by the two coupled equations , , is iteratively solved having assumed a tentative nodal gas composition $\mathbf{C} = \{\mathbf{c}_i\} \in \mathcal{R}^{N_{\text{G}},\kappa}$.

Once having converged on the fluid-dynamic state of the gas network the model addresses the gas quality problem. The mass balance is performed assuming each node as control volume and it is carried out for each chemical species by applying the mass concentration vectors to the continuity equation (9). The mass balance detailed for each chemical species takes the following matrix form:

$$\left(\boldsymbol{X}_{\text{G}_+}^{\text{T}} \,\text{diag}(\mathbf{g})\, \boldsymbol{X}_{\text{G}} + \text{diag}\left(|\mathbf{g}_{\text{ext}_+}|\right) \right) \mathbf{C} = -\text{diag}\left(|\mathbf{g}_{\text{ext}_-}|\right)\, \mathbf{C}_{\text{ent}} \tag{14}$$

where $\boldsymbol{X}_{\text{G}_+}$is the positive part of the incidence matrix $\boldsymbol{X}_{\text{G}}$, $\mathbf{g}_{\text{ext}_+}$ and $\mathbf{g}_{\text{ext}_-}$ are the positive and the negative part of the vector $\mathbf{g}_{\text{ext}}$ respectively (thus the outlet and the inlet gas flows).

The nodal concentrations $\mathbf{C}$ are determined by solving the linear set of equations (14), updating the gas composition at each node of the network. This may change the properties according to which the previous fluid-dynamic problem has been solved. Because of this reason, an additional iterative procedure is carried out until convergence, to solve the multicomponent fluid-dynamic problem. In case of multiple injection points, which introduce gases with different compositions, the model is then able to keep track of the composition variation throughout the network, taking into account the variations on the fluid-dynamic properties of the mixture as well as the calorific value.

2.6 Interlink between the infrastructure models

The integrated modelling framework consists of the simulation of the electricity and the gas network infrastructures in a successive time steps. The networks integration strategy addressed with this case study does not generate an interdependency between the electrical and the gas system but rather links the electrical energy over-production to the gas network by means of hydrogen production and injection, with no further impacts caused by the gas network to the electricity one. For this reason, there is no need to set up a proper co-simulation modelling framework (capable to solve numerically power and gas flows within the same time iteration) but it is sufficient to perform a consequential modelling.

The complete modelling framework is depicted in the flow chart of Figure 1.

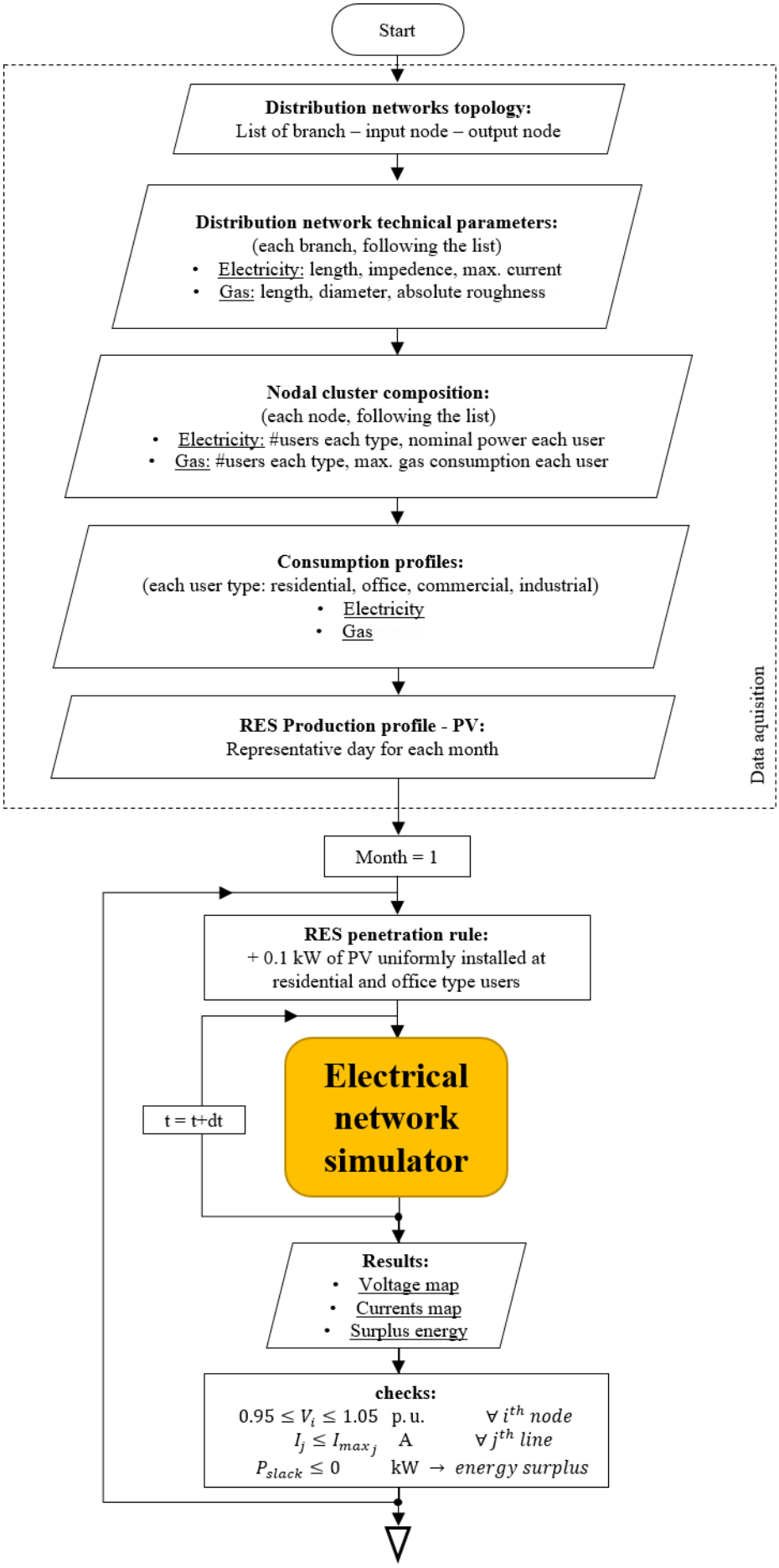
Start
Distribution networks topology:
List of branch – input node – output node
Distribution network technical parameters:
(each branch, following the list)
• Electricity: length, impedence, max. current
• Gas: length, diameter, absolute roughness
Nodal cluster composition:
(each node, following the list)
• Electricity: #users each type, nominal power each user
• Gas: #users each type, max. gas consumption each user
Consumption profiles:
(each user type: residential, office, commercial, industrial)
• Electricity
• Gas
RES Production profile - PV:
Representative day for each month
Data aquisition
Month = 1
RES penetration rule:
+ 0.1 kW of PV uniformly installed at residential and office type users
Electrical network simulator
t = t+dt
Results:
• Voltage map
• Currents map
• Surplus energy
checks:
$0.95 \leq V_i \leq 1.05$ p.u. $\forall\, i^{th}\ node$
$I_j \leq I_{max_j}$ A $\forall\, j^{th}\ line$
$P_{slack} \leq 0$ kW $\rightarrow$ $energy\ surplus$

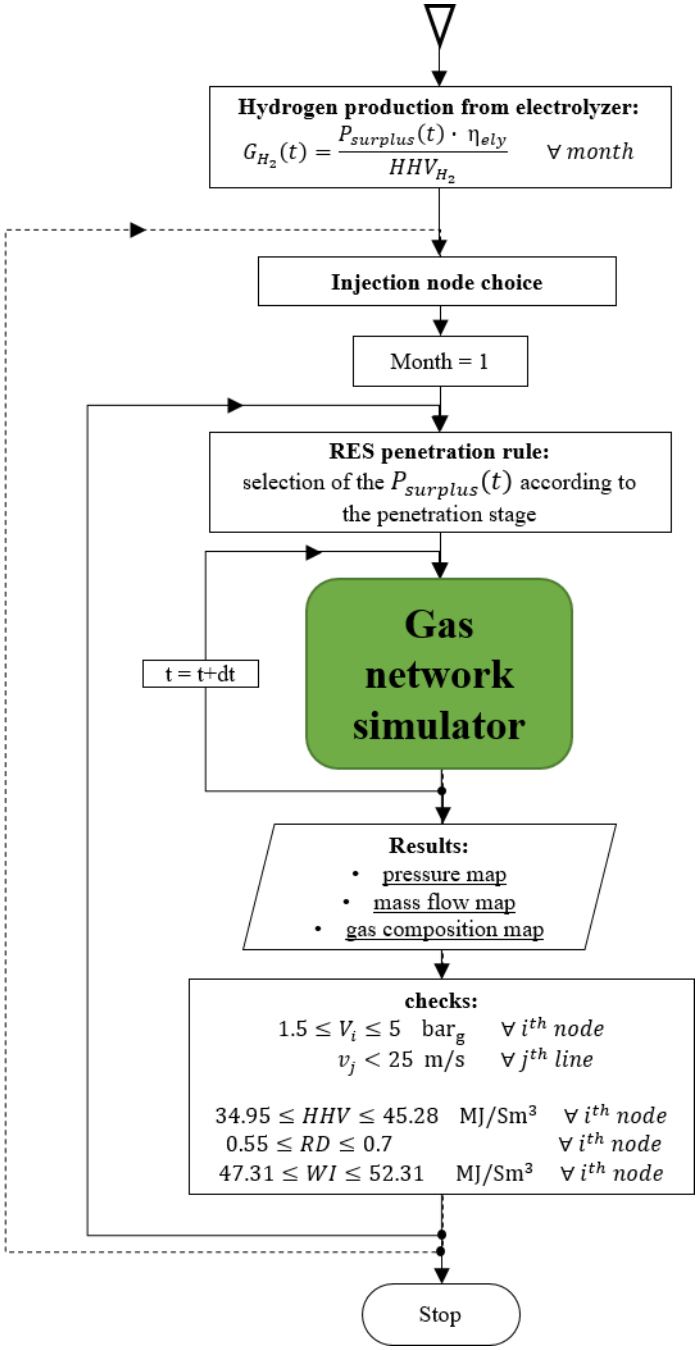

Figure 1 – Flow chart of the complete consecutive modelling framework.

At first, all the data about the energy infrastructures and the energy consumption profiles are collected. The topology of the networks as well as the useful technical features of the branches (lines and pipelines) are provided to the model as parameters. Being the medium voltage and medium pressure level of the energy grids the focus of the model, the majority of the consumption nodes are composed of groups of users. The composition of each consumption group in terms of types of final users is also an important information to be given. The data acquisition phase ends with the input of the power and gas consumption curves for each user

type. In this specific case, these data are obtained from users' consumption profiles expressed as a fraction of the installed electrical power and the daily gas flow rates.

The RES penetration scenario is then tested on the electricity infrastructure. A RES penetration rule is decided so that distributed generation is progressively installed. For each installation step, the electric power flow calculation is performed for a typical day by means of the electrical network model. Photovoltaic production curves for a typical day of each month, taken from PVGis database [66] are also provided as input to the model. In fact, to take into account the seasonality of the photovoltaic production, a further month-by-month iteration is carried out.

In order to check the operating conditions of the electric infrastructure, specific performance indicators are calculated and their compliance with the normal operation limits are checked. Table 1 summarises the performance indicators considered for the electrical case, together with their operational limits.

Table 1 – Normal operational limit for the electricity distribution network considered in this work.

Parameter	**units**	**Limit**
Nodal voltages	[p.u.]	0.95 – 1.05
Maximum current	[p.u.]	< 1
Reverse power flow	[p.u.]	0

Thus, possible deviations of the performance indicators are assessed, and a system integration strategy is developed in order to solve the issues emerged. The incorporation of P2G is assumed: a photovoltaic overproduction curve may be produced whenever a deviation from normal operating condition occurs. This curve is supplied to the electrolyser model, which converts it into a hydrogen production rate, acting as an additional electric load. . In general, the overproduced electricity is fed back to the medium voltage distribution grid and the P2G location on the electrical infrastructure is chosen so to solve the detected issues. The injection node choice comes afterwards by selecting the nearest node on the gas network. The produced hydrogen is injected directly in the gas distribution infrastructure so that it is blended within the natural gas stream. The gas network model is run and the effects of the variation of gas composition in time and in space are evaluated. Also for the gas case, the operating conditions of the infrastructure are checked. Fluid-dynamic indicators and

their compliance with the normal operation limits are evaluated. The limit on the gas velocity is required in order to avoid noise and dragging phenomena of impurities. Furthermore, the three main parameters for the evaluation of the gas quality are also considered. These parameters are the most common throughout all the European regulations and standards [67]. Table 2 summarises the performance indicators considered for the evaluation of the gas network case, together with their operational limits referred to the Italian case [68] which does not foresees any hydrogen as a component of natural gas.

Table 2 – Fluid-dynamic operational limits for medium pressure (4th species) distribution network and Italian national gas quality ranges [68].

Parameter	**Units**	**Limit**
Pressure	[bar_g]	1.5 – 5
Gas Velocity	[m/s]	< 25
Higher Heating Value	[MJ/Sm^3]	34.95 – 45.28
Relative Density	[-]	0.55 – 0.7
Wobbe Index	[MJ/Sm^3]	47.31 – 52.31

3 Case Study Description

The case study aims to show the potentials of an integrated modelling approach taking as example the distribution systems in an urban context. The urban area is built around the available data for an urban electrical grid, with topology and technical features coming from the *Atlantide* project [69]. The aim of the project was to create a repository of reference electrical distribution networks (low and medium voltage) characterized by representative technical parameters, load type distribution and clustering, as well as providing typical consumption profiles for each load type. Starting from an urban-type set of data, the electrical scheme was shaped in a topographical form covering an area of 4.4 × 5 km^2. The spatial distribution of the users, together with the estimation of their gas consumption rates, allowed designing a possible gas network layout, consistent

with the urban framework associated to the electrical case [70]. In the following sections, the main features of the two infrastructures as well as the related consumption localization and profiles are given.

3.1 Electrical infrastructure

The electrical grid is operated at medium voltage (15 kV) and consists of one supply (slack) node, 96 other nodes and 96 lines, composed of 11 feeders (from F_1 to F_11) with radial connection (Figure 2). All the lines are described in terms of linear resistance, capacitance and inductance, as well as length and maximum current. Each node may be either a final user or an aggregation of users. No distributed generation is present in the base case.

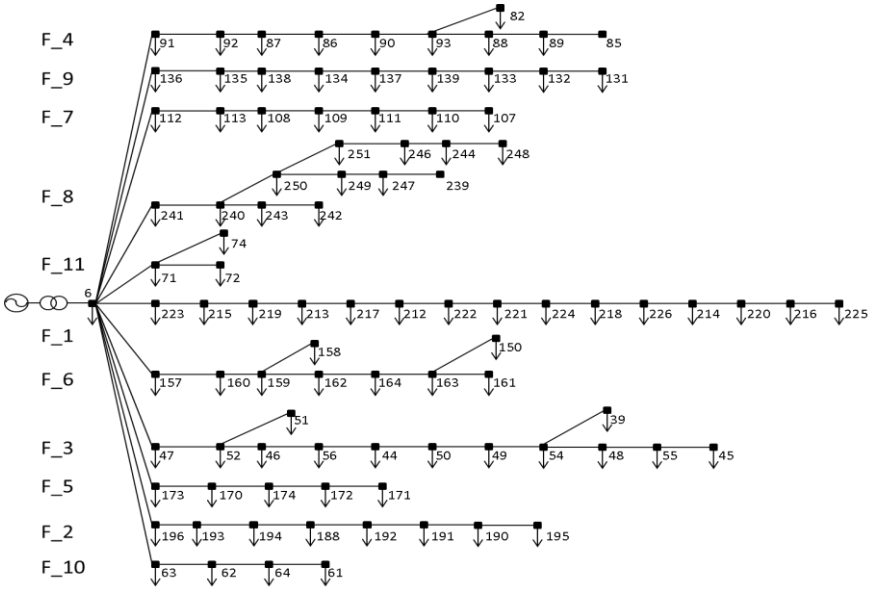

Figure 2 – Schematic topology of the urban electrical distribution network.

3.2 Electrical user types, rated power and profile

Four categories of users are considered in this framework: residential, industrial, commercial and offices. The nodes along each feeder may be either industrial users directly connected to the MV network, or MV/LV substations supplying through radial LV systems the other types of consumers (not represented in the schematic). For every node, the total installed rated power related to the load types is known. Assuming a set of reference nominal powers for each users' counter, it was possible to determine the number of users for each

category as well as estimate the number of inhabitants. The total power load is 25.6 MW_e and on the basis of the assumptions made, the inhabitants are about 11,500.

Concerning the users' profiles, 4 load curves were available from [69], one for each category, with a time step of 15 min. These load profiles are taken from representative cases that refer to loads found in the same type of electrical distribution network. Figure 3 shows the profiles expressed in p.u. with respect to the installed power.

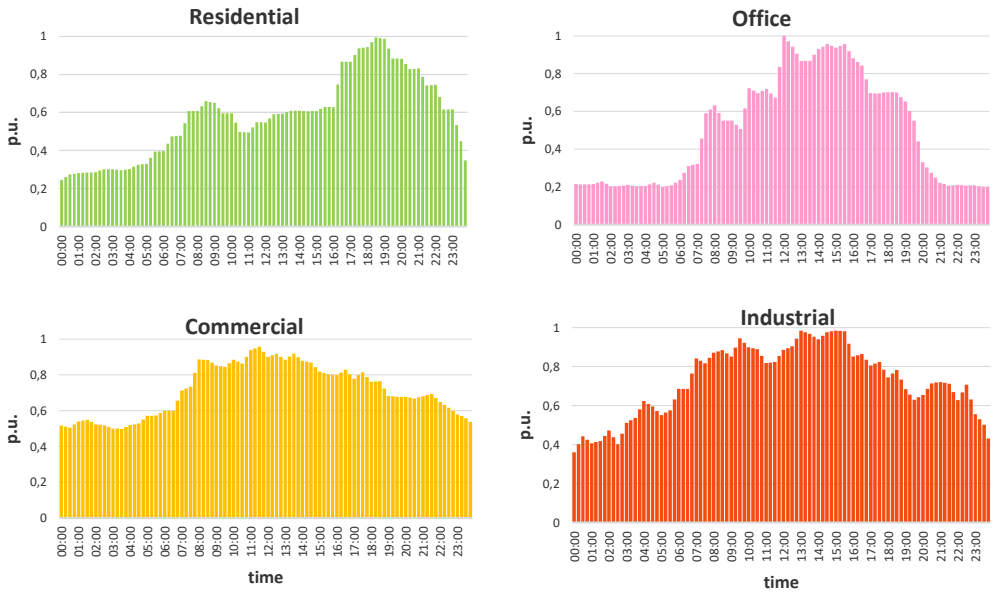

Figure 3 – Electricity consumption profiles for each user type.

As the last step towards the characterization of the sample urban area, a topographic shape of the scheme in Figure 4 is proposed by choosing a spatial resolution of 0.1 x 0.1 km where to distribute the number of users clustered at each node of the electrical network. In particular, for what concerns residential users, a set of three different densities was considered [70]. In this way, a gas network may be designed accordingly, after having estimated the gas consumption of the scattered users. On the left-hand side, the topography of the urban area is shown, while on the right-hand side the layout of the gas network is presented.

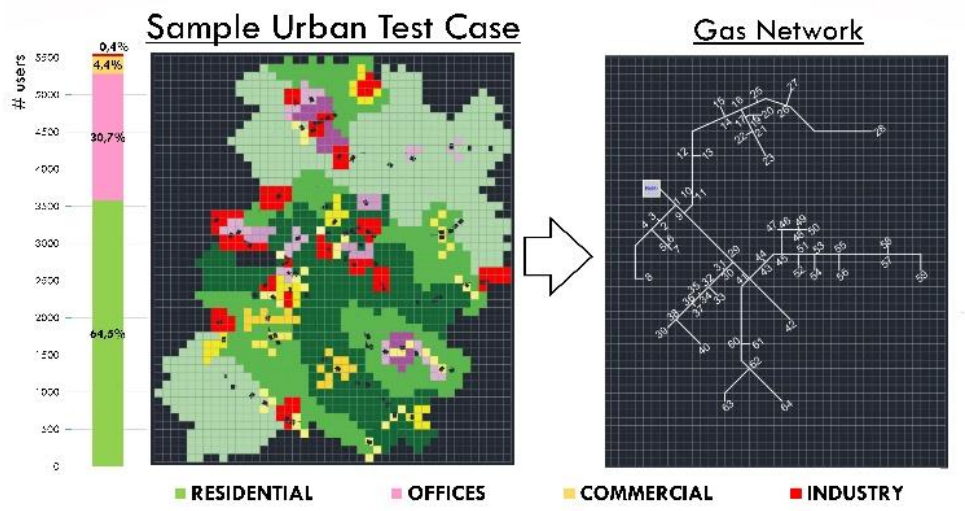

Figure 4 – Urban case topography and proposed gas network layout.

3.3 Natural gas infrastructure

The natural gas infrastructure was designed on-purpose, starting from the available data and information from the electrical case and estimating the maximum possible hourly flow rates [70]. Natural gas networks are usually operated on multiple pressure levels, ranging from $p > 24$ $\mathrm{bar_g}$ for the transmission backbones to $p \leq 0.04$ $b\mathrm{ar_g}$ for the pipelines reaching the majority of the final users. As for the Italian case, the classification of the pressure levels is set by law in [71]. Concerning the distribution domain, most of the gas networks are structured on two pressure levels: a medium pressure one (e.g. $p \in [1.5 \div 5]$ $\mathrm{bar_g}$ – 4$^{\mathrm{th}}$ species) distributing gas mainly to industrial users and clusters of smaller final users through Final Reduction Stations (FRSs). These stations reduce pressure to the lower level feeding the final sections of the infrastructure ($p \in [0.5 \div 0.04]$ $\mathrm{bar_g}$ – 6$^{\mathrm{th}}$ species or lower). Following the approach of the electrical case, the addressed gas network is the medium pressure one, operated at $p_{max} = 5$ $\mathrm{bar_g}$ (4$^{\mathrm{th}}$ species). It has a tree-like topology, consisting of 64 branches and 63 nodes, a fraction of whom are consumption ones. Among them, 22 nodes consist of industrial users directly connected to the medium pressure network, and 12 nodes are FRSs, feeding non-industrial areas of consumption. As shown in Figure 4, the network starts from a single metering station (M/R station), also called city-gate, located outside the urban context limits, in which gas from the transmission level is withdrawn. It is composed of a central feeder that supplies five other sub-feeders to the FRSs or industrial users. All the pipe sections are described in terms of inner diameter, length and inner roughness.

3.4 Natural gas user types, rated power and profile

The gas consumption data have also been estimated starting from the electrical case. As a fundamental assumption, it was decided that for each single electrical user, a gas counter is installed, to have an equivalence between electrical and gas users, keeping the distinction among the four categories as in the previous case. For each users' category, the natural gas consumption estimation was carried out through semi-empirical methodologies [72], commonly used within the gas sector. Daily gas consumption data per unit of building covered area (or covered volume) were available from handbooks [73] so the daily consumption was calculated assuming covered areas and volumes for each user category. The daily consumption of natural gas is the starting value both for the calculation of the maximum gas flow (useful to size the gas network) and for the gas consumption profiling (in order to run the simulations). Concerning natural gas uses for the industrial activities, the allocation of the consumption of each user was carried out arbitrarily choosing the industrial sector to which it may belong, then determining the related typical yearly consumption. According to this methodology, the total consumption of natural gas on yearly basis is about 100.3 MSm^3/y.

Concerning the users' gas consumption profiles, the curves in Figure 5 are proposed as own elaboration based on the four electrical load curves already presented and other available consumption patterns in [73] and [72]. As for the industrial users, two profiles have been considered: a space heating one (obtained following the same assumptions just mentioned) and a technological process one. The latter has been considered as a simply flat profile throughout the day as if industrial processes would require continuous gas supply. The time step is equal to 15 min, and the data are expressed as a percentage of the daily consumption.

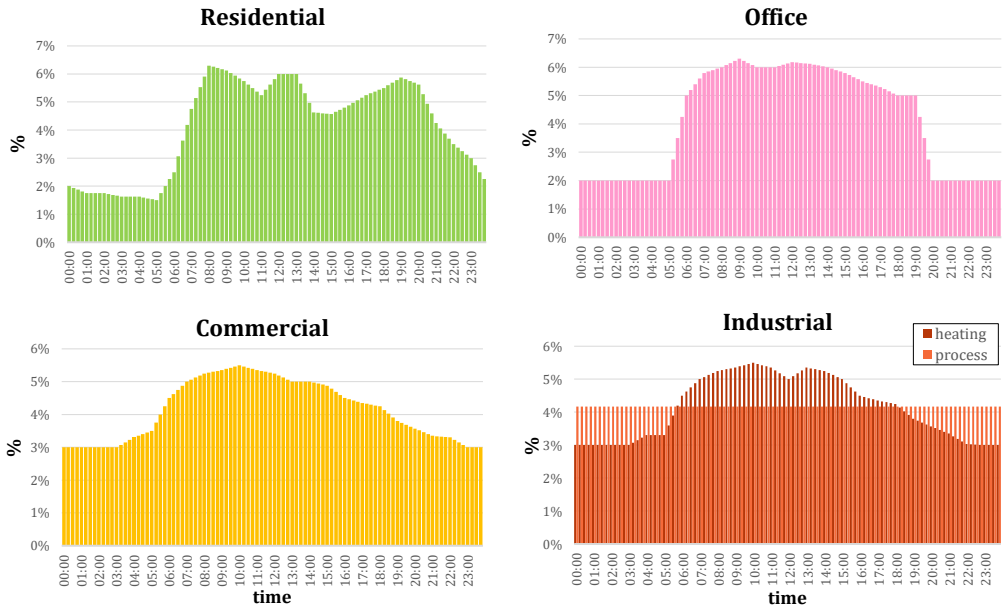

Figure 5 – Natural gas consumption profiles for each user type.

Table 3 summarises the main electricity and gas statistics of the area, in terms of the allocation of the installed power among the four users' categories, their yearly gas consumption and their share over the total number of users.

Table 3 – Electricity statistics of the urban area according to users' type in terms of distribution of the installed nominal power and of the users' type.

	total	**Residential**	**Commercial**	**Industrial**	**Offices**
Installed power	25.6 MW_e	42 %	13 %	15 %	30%
Gas Consumption	100.3 MSm^3/y	5.9 %	14.3 %	69.5 %	10.2 %
Number of users	5,547	64.5 %	4.4 %	0.4 %	30.7

4 Simulations and Results

4.1 Increasing of photovoltaic distributed generation

RES penetration has been assumed to be progressive, meaning that installations are incremental. For each installation step, a new 0.1 kW photovoltaic power was installed at each node with residential and office type users. Thus, installations result evenly distributed throughout the nodes and their size is linearly increasing.

For each iteration, the electrical network is simulated over the whole year considering 12 representative days. The performance indicators are checked for the whole time period. The voltage at each node is always maintained within the operational limit. Conversely, the thermal limit is exceeded for the first time in the case of 12.1 kW of photovoltaic power plant installed at each residential and office user, corresponding to a scenario of a solar energy penetration (i.e. annual photovoltaic energy production divided by the total energy consumption) equal to 106.7%. More specifically, the saturation period lasts just for a single time step (15 min), taking place only in July and the saturated line is line 1 – the branch collecting all the feeders towards the HV/MV transformer. As of reverse power flow, Figure 6 depicts the evolution of the net consumption of active power for the whole urban area (i.e. the active power exchanged at the HV/MV substation) as the solar penetration increases. Each line refers to a photovoltaic installation case to which corresponds a certain level of solar energy penetration (as indicated in the legend). The two sets of lines refers to the winter case (February – left) and the summer case (July – right). As the distributed solar energy increases, the net exchange of active power at the substation decreases until reaching negative values. In these cases, a reverse power flow is registered at the substation, meaning that the urban area is able to export energy to the high voltage transmission level of the power network. Following the rationale of this case study, the surplus energy profile (the negative portion of the curves in Figure 6) is to be converted to a hydrogen flow rate by P2G.

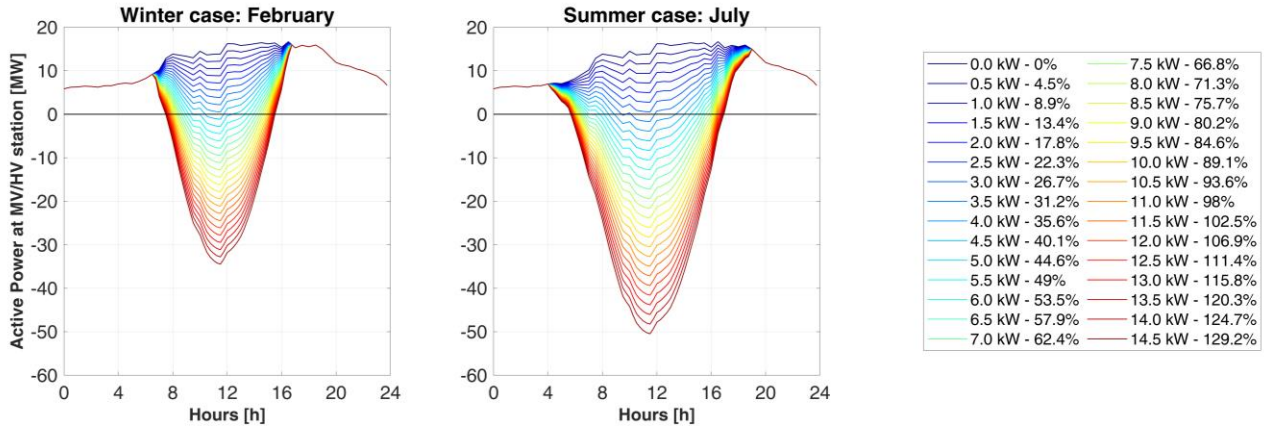

Figure 6 – Net active power flow exchange at MV/HV station under increasing share of distributed energy generation from photovoltaic. Positive values represent the total consumption of the urban area. Negative values indicates a net surplus of solar energy production within the area. Left: representative winter case (February); right: representative summer case (July). The legend reports the percentage of PV energy production over the total energy consumption (on annual basis).

The reverse power flow condition occurs for the first time when the photovoltaic penetration corresponds to 27.6% of the total energy consumption (3.2 kW installed at each user). The first occurrence is recorded for

one hour during the month of July, for a total energy surplus of 244 kWh with maximum surplus power of 344 kW. In order to observe reverse power flows all year round, the photovoltaic penetration must have reached 53.5%. (6.1 kW installed each users). In this case, occurrences range from 30 minutes for a typical day of December to 8 hours 15 minutes in July. In Figure 7, the evolution of the occurrence of the reverse flow condition is given as a function of months and of the penetration of photovoltaic energy on the total consumptions of the area. In this case reverse flow occurrences are evaluated in terms of percentage of hours in which the reverse flow takes place over the whole year (z-axis values).

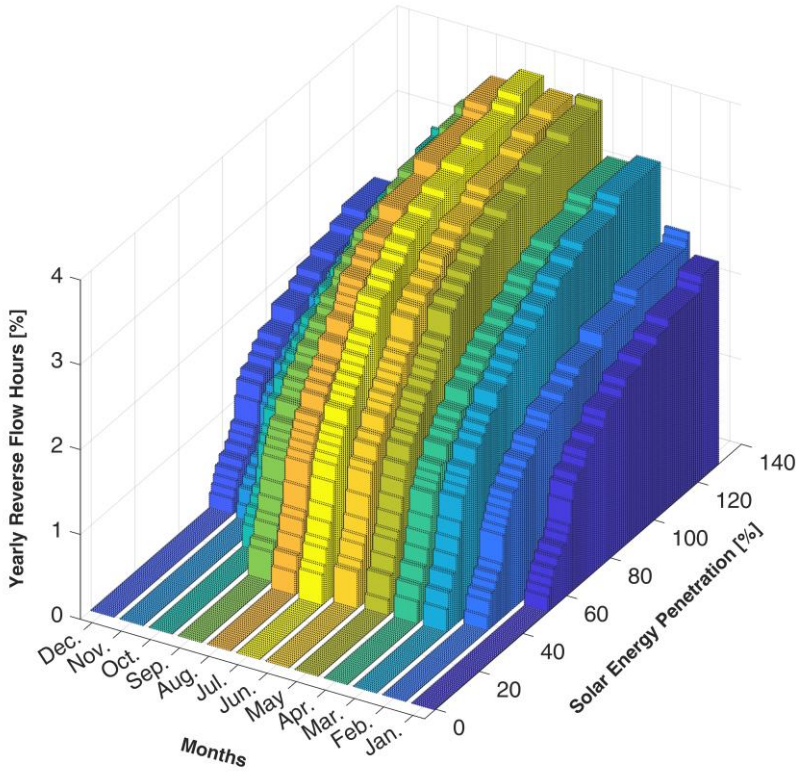

Figure 7 – Occurrences of the reverse flow condition is given as a function of months and of the penetration of photovoltaic energy (i.e. annual photovoltaic energy production divided by the total energy consumption). Reverse flow occurrences are evaluated in terms of percentage of hours in which the reverse flow takes place over the whole year (vertical axis values)

4.2 Electricity and gas sector coupling

The electrical simulation above shows that the main deviation from the normal operating conditions consists of the occurrence of reverse power flows, whose frequency and intensity increase as the photovoltaic

energy production increases. Even though it is not as critical as a deviation of nodal voltages or the overloading of the lines, it implies, with respect to the higher voltage levels of the network, the transformation of a passive hub to an active one, providing energy rather than consuming it. In order to avoid this situation, the energy surplus may be stored locally. A strategy of sector coupling is here proposed by considering a power-to-gas solution based on an electrolyser, which produces hydrogen whenever a surplus of power is available from the grid. The power to hydrogen efficiency is assumed equal to $70\%_{HHV}$ as commonly reported in the literature [74], [75] and reflecting the actual conversion efficiencies of a polymeric electrolyte electrolyser cell. The hydrogen production profile is then calculated accordingly, assuming a fully flexible operation (0 – 100% of the installed power). Solid lines in Figure 8 shows the hydrogen production patterns for three different levels of photovoltaic energy penetration (30%, 40%, 50%), both for the summer case (July) and for the winter case (February). In view of the injection of hydrogen within the natural gas stream, it is worth mentioning that the seasonality affects also the gas network, being the gas demand tightly related with the space heating needs. To take this into account, the gas consumption profiles in the summer case have been reduced to the 15% of the winter case (with the exception of the process-related industrial gas consumption profile). This reduction is consistent with the allocation of the daily consumption indicated by the Italian Authority [76].

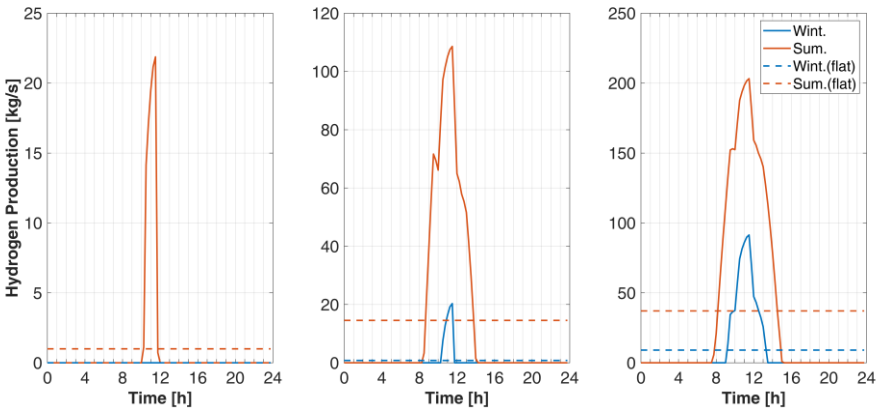

Figure 8 – Hydrogen production patterns for three different stages of photovoltaic energy penetration (30% 40% 50% from left to right). Orange lines: summer case (July); Blue lines: winter case (February). The dashed lines are the corresponding flat injection profiles.

4.3 Hydrogen injection scenarios

A wide range of variability characterizes hydrogen injection scenarios depending on several parameters. In the framework of hydrogen blending within the gas network infrastructure, two additional terms of variation may be considered:

1) the “direct injection” versus the “flat injection”;

2) the choice of the injection node.

The first condition considers the possibility to decouple the hydrogen production profiles with the injection ones by means of a suitable buffer system. Thus, for each of the five injection profiles in Figure 8, a corresponding “flat profile” over the whole day is generated (dashed lines). These profiles will be applied to run the simulations of distributed injection on the network infrastructure in order to test the impact of this type of sector coupling. Concerning the choice of the injection node, all the hydrogen production profiles are tested on two different injection nodes. In the first case, an intermediate node (node 30) is chosen, following a proximity criteria between the HV/MV station and the gas network. In the second case, the hydrogen injection is assumed to be localized right after the gas city gate (node 2).

For each of the three stages of photovoltaic energy penetration, four injection profiles have been generated, considering the seasonal variation (summer or winter) and the injection mode (direct or flat). In addition, these injection scenarios have been tested on two different injection nodes, thus generating a total of 24 hydrogen injection scenarios.

4.4 Hydrogen injection results

In this paragraph, the results of the fluid-dynamic simulations of the 24 hydrogen injection scenarios are reported and compared. Hydrogen injection within the gas infrastructure has an impact both on the fluid-dynamic of the gas flowing within the pipelines and on its composition and quality. Furthermore, dealing with network systems and distributed injections, the gas properties vary throughout the network and the magnitude of the introduced perturbation varies according to the injection point.

4.4.1 Fluid-dynamic results

Under a fluid-dynamic point of view, the main quantities to be analysed are the gas velocity along each pipeline (< 25 m/s as reported in technical codes of distribution gas networks) and the pressure level at each node (between 1.5 – 5 bar_g). For each injection scenario and for each modelled time step, these quantities have been compared with their operational limits in order to check the fluid-dynamic impacts of blending hydrogen within the natural gas. Results show that gas velocity may exceed the maximum value in a few branches during

a few hours of the winter case, when the hydrogen injection rate is one of the highest. The critical cases refer to the highest photovoltaic penetration stage (50%) when considering the direct injection mode. However, they do not correspond to the highest hydrogen injection rate, since the maximum is produced during the summer season. This means that the exceeding of the gas velocity limit is not directly linked to the amount of hydrogen injected, but is rather caused by a combined effect of hydrogen flow rate and higher natural gas consumption, as it will be clarified afterwards. Concerning pressure levels, no criticalities emerge. Figure 9 provides a comprehensive visualization of the gas network fluid-dynamic status for the two injection-node cases. A single timeframe of a specific injection scenario needs to be selected. The 10:45 timeframe of the 50% photovoltaic penetration – winter case is selected as one of the most critical.

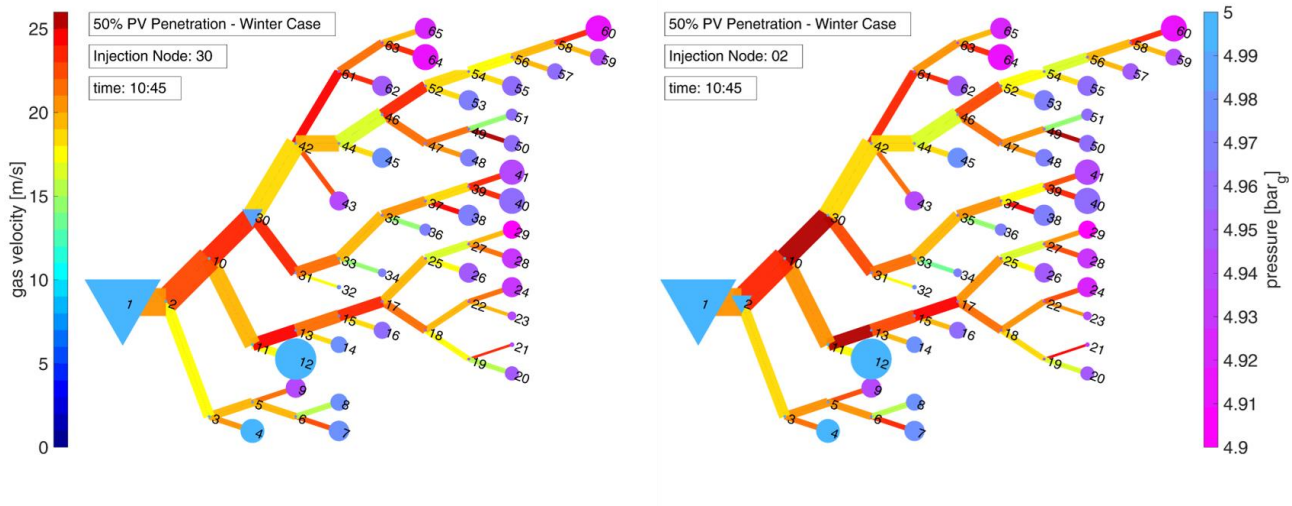

Figure 9 – Comprehensive gas network visualization of fluid-dynamic results for a specific time step of the 50% photovoltaic penetration – winter case. Left: injection node 30 – right injection node 02

Considering that the amount of injected hydrogen is the same for the two cases, it can be inferred that the choice of the injection node has an impact on the velocity field throughout the network branches. When hydrogen is injected at node 30, just one branch undergoes gas velocities higher than 25 m/s (branch 49). Conversely, in the case of node 02 as the injection one, the impact on the network is wider: the branches with exceeding velocities are three (branches 12, 29, and 49). For both cases branch 49 results to be the critical one. Figure 10 represents the daily velocity profiles within branch 49 and it is given in order to evaluate the effects on the gas velocity of the different amounts of hydrogen that are obtained for all the scenarios of direct injection during different seasons and for both the injection-node cases.

Figure 10 helps to clarify the combined effect of hydrogen abundance and higher natural gas consumption that leads to the exceeding gas velocity within branch 49. While gas velocity perturbation is smaller among the winter cases than the summer ones due to the smaller hydrogen production rate, the gas velocity within the pipelines is sensibly higher because of the higher gas consumption. Furthermore, by the comparison of the two injection-node cases of Figure 10, it can be noted that injecting hydrogen in node 30 (intermediate node) has higher impacts on the velocity than injecting at node 02, because the same amount of hydrogen is injected within a smaller amount of natural gas stream. This also has an impact on gas quality perturbation, as commented below.

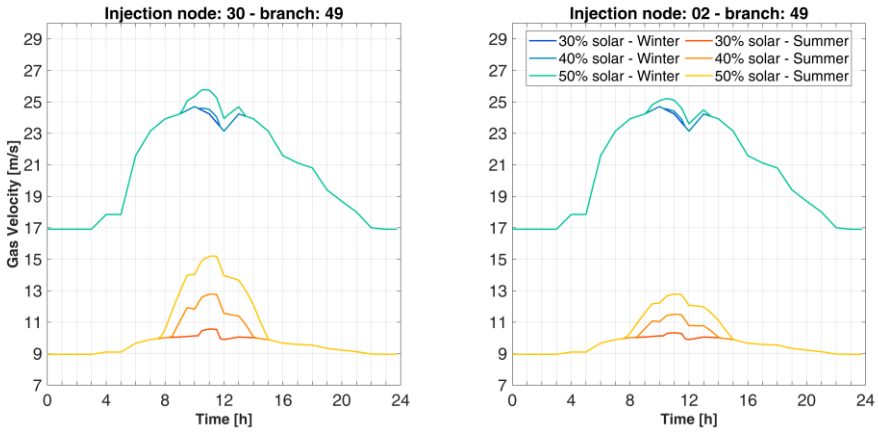

Figure 10 – Daily velocity profiles within branch 49. Left: injection node 30 – right injection node 02.

A quantification of the velocity perturbation induced by the distributed injection of hydrogen at different nodes of the network and for the different seasons is given in Figure 11.

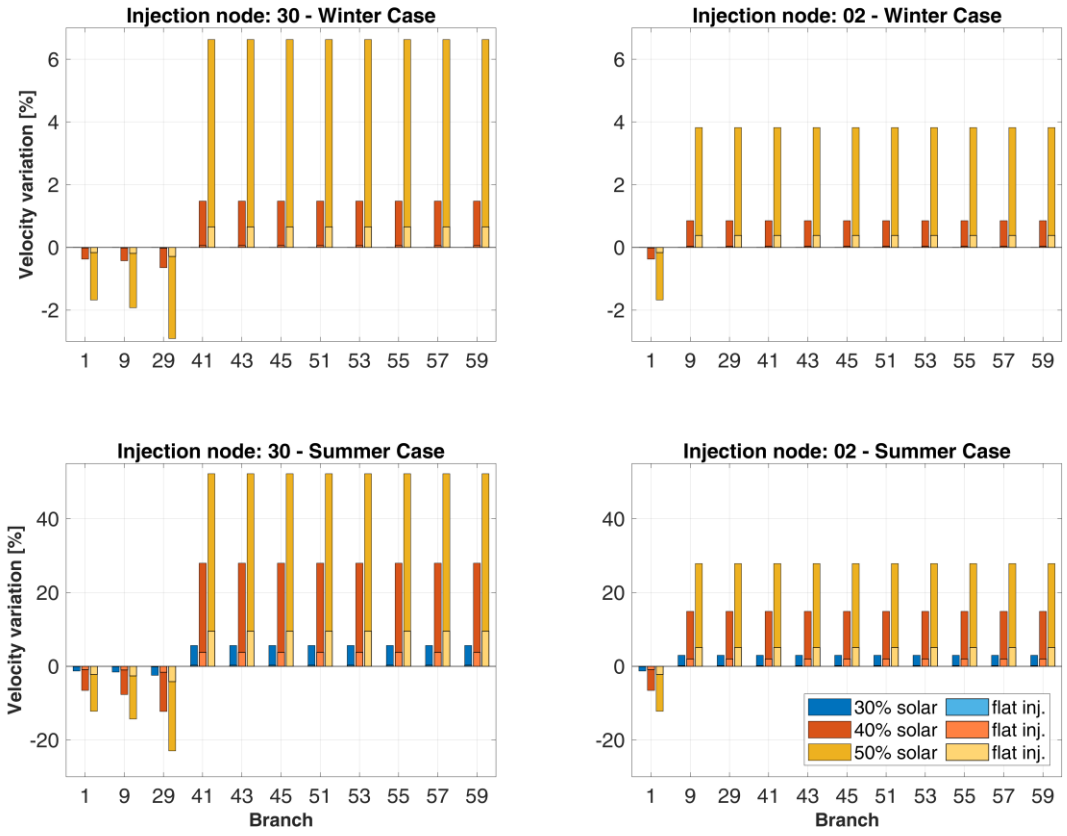

Figure 11 - Velocity perturbation induced by the distributed injection of hydrogen with respect to the no-injection case (base case) along the longest branch of the network. Left: injection node 30 – right injection node 02; upper part: winter cases, lower part: summer cases; lighter colours: flat injection cases.

The variation is calculated in relative terms with respect to the base case (gas network operated with no distributed injections). All the graphs refer to the same sequence of branches, from the gas city gate to the farther node of the network (node 60). Data refer to the time step characterized by the maximum hydrogen injection rate (t=11:30). All the three hydrogen injection profiles coming from the three levels of photovoltaic penetration are reported, as well as the related flat injection cases (bars in lighter colour). To be noted that for the 30% photovoltaic penetration case, no hydrogen is produced during the winter months, so no perturbations are detected. It is also worth noting that scales are different thus in the case of 50% of photovoltaic penetration, the velocity increase downstream the injection nodes ranges between almost the 4% to more than 50%. The highest perturbations occur for the summer cases and for the intermediate injection node (node 30). The same behaviour is to be found for the flat injection cases, even though the perturbations are sensibly lower: from less than 1% to slightly more than 5%. As a final remark, Figure 11 also depicts a difference in the sign of the

velocity variation. Gas velocities increase downstream the injection and decrease upstream the injection as a result of the substitution of an amount of natural gas with an unconventional fuel gas (hydrogen) that has a lower calorific value on a volume basis (HHV_{H2} = 12.07 MJ/Sm^3 ; HHV_{CH4} = 37.09 MJ/Sm^3).

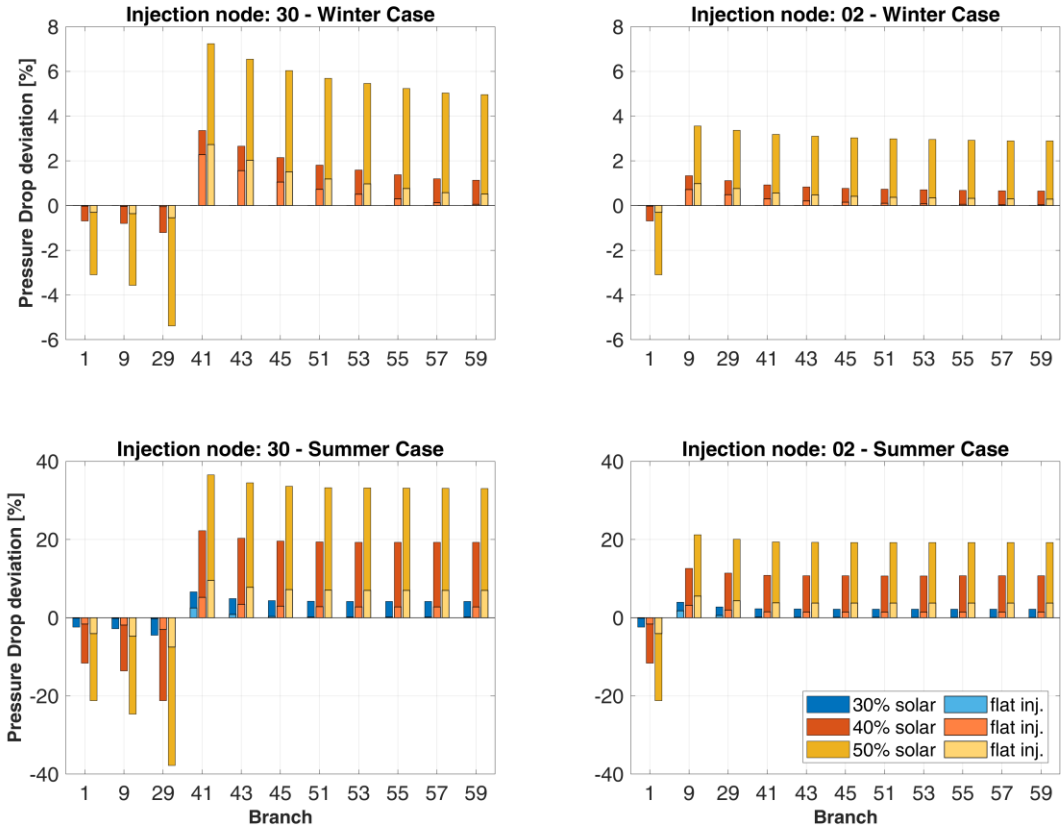

Figure 12 – Pressure drop perturbation induced by the distributed injection of hydrogen with respect to the no-injection case (base case) along the longest branch of the network. Left: injection node 30 – right injection node 02; upper part: winter cases, lower part: summer cases; lighter colours: flat injection cases.

The variation of volume gas flows has also an impact on the pressure drops along the pipelines. Figure 12 shows the pressure drops variation with respect to the base case along the same sequence of branches as in Figure 11 and for the same time step. All the three hydrogen injection profiles coming from the three stages of photovoltaic penetration are reported, as well as the related flat injection cases (bars in lighter colour). Pressure drops variations follow the same trends as the velocities ones; however, the impact on the pressure levels at each node is negligible, as it can be inferred from Figure 13.

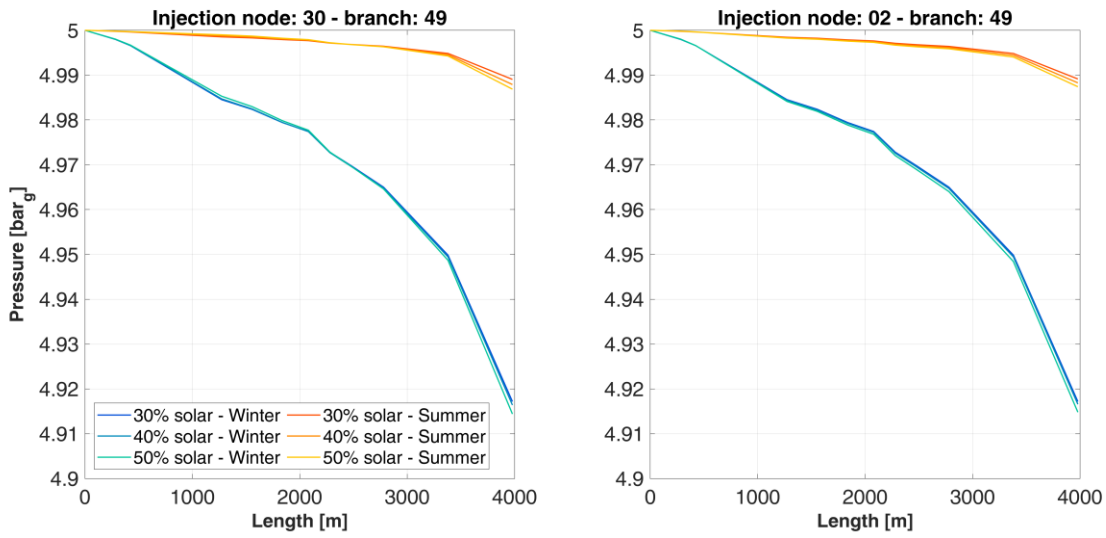

Figure 13 – nodal pressure along the longest branch of the network. Left: injection node 30 – right injection node 02; blue curves: winter cases, orange curves: summer cases.

The pressure profile along the selected sequence of branches is given. Nodal pressures are given with respect to the distance from the starting node (city gate) so to picture the pressure profile as a function of the cumulative length. For each node-injection case, pressures profiles are given for the direct injection case for all the three stages of photovoltaic penetration, both for the winter and for the summer case. It is evident that pressure levels are negligibly affected for any of the addressed scenarios.

4.4.2 Gas quality results

The major impact of hydrogen injection practice within natural gas infrastructure is on gas quality parameters. The three main parameters, together with the hydrogen molar concentrations are presented in Figure 14 and Figure 15 for all the addressed case studies. The graphs display the variation of the quality parameters for the whole day and for all the injection cases related to a specific photovoltaic penetration stage. Figure 14 shows the direct injection cases while Figure 15 refers to flat injection ones. Orange curves refer to summer cases while the blue ones to the winter season. For each season, the injection cases at node 30 and at node 02 are given, thus resulting in four curves for each graph. Concerning the higher heating value, the relative density and the Wobbe index graphs, the higher and the lower limits of acceptability, as expressed in the Italian Standard [68], are also depicted, delimiting the acceptability area (colored area).

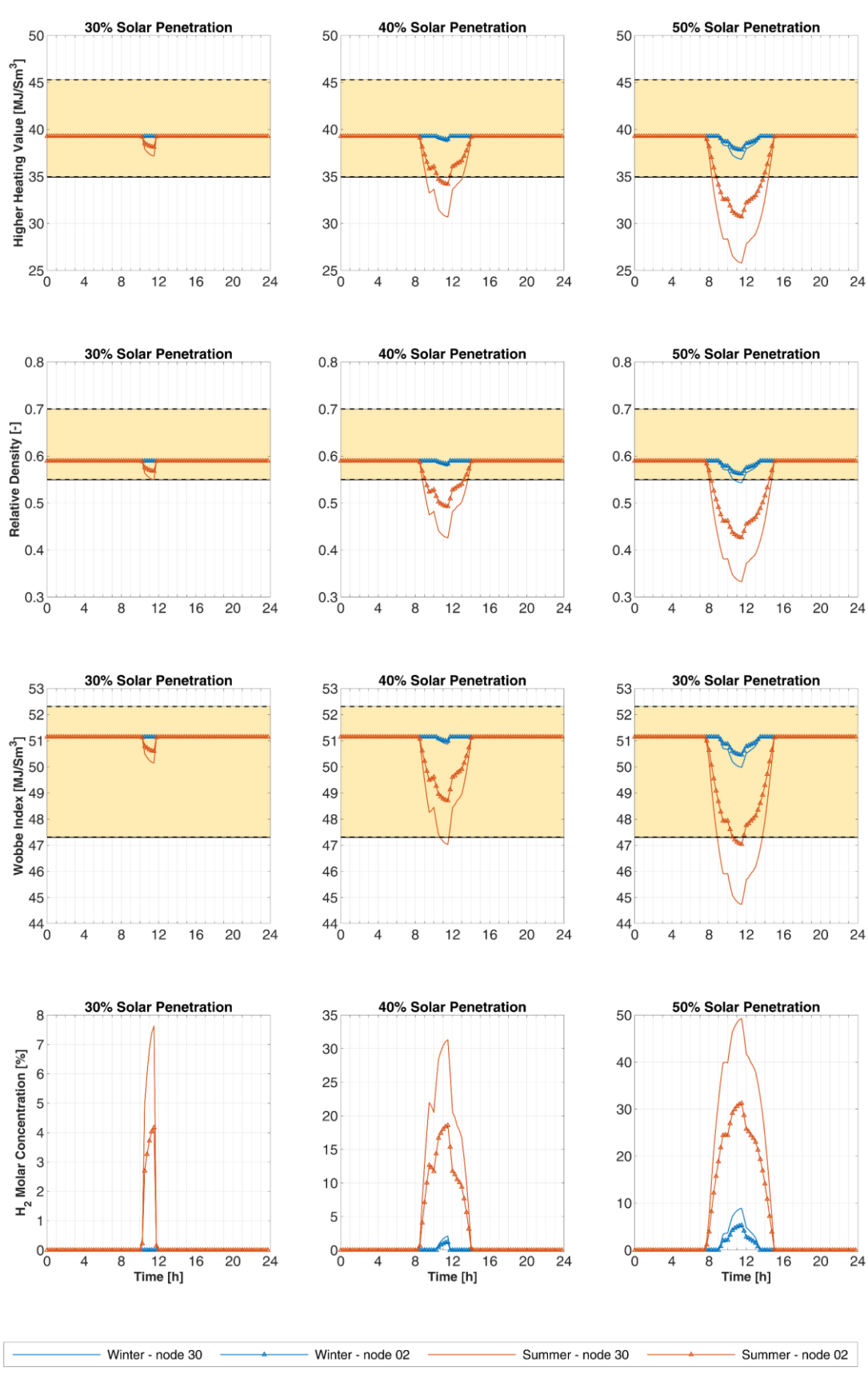

Figure 14 – Daily variation of gas quality parameters and hydrogen molar concentration for the complete set of injection scenarios, under the assumption of direct injection.

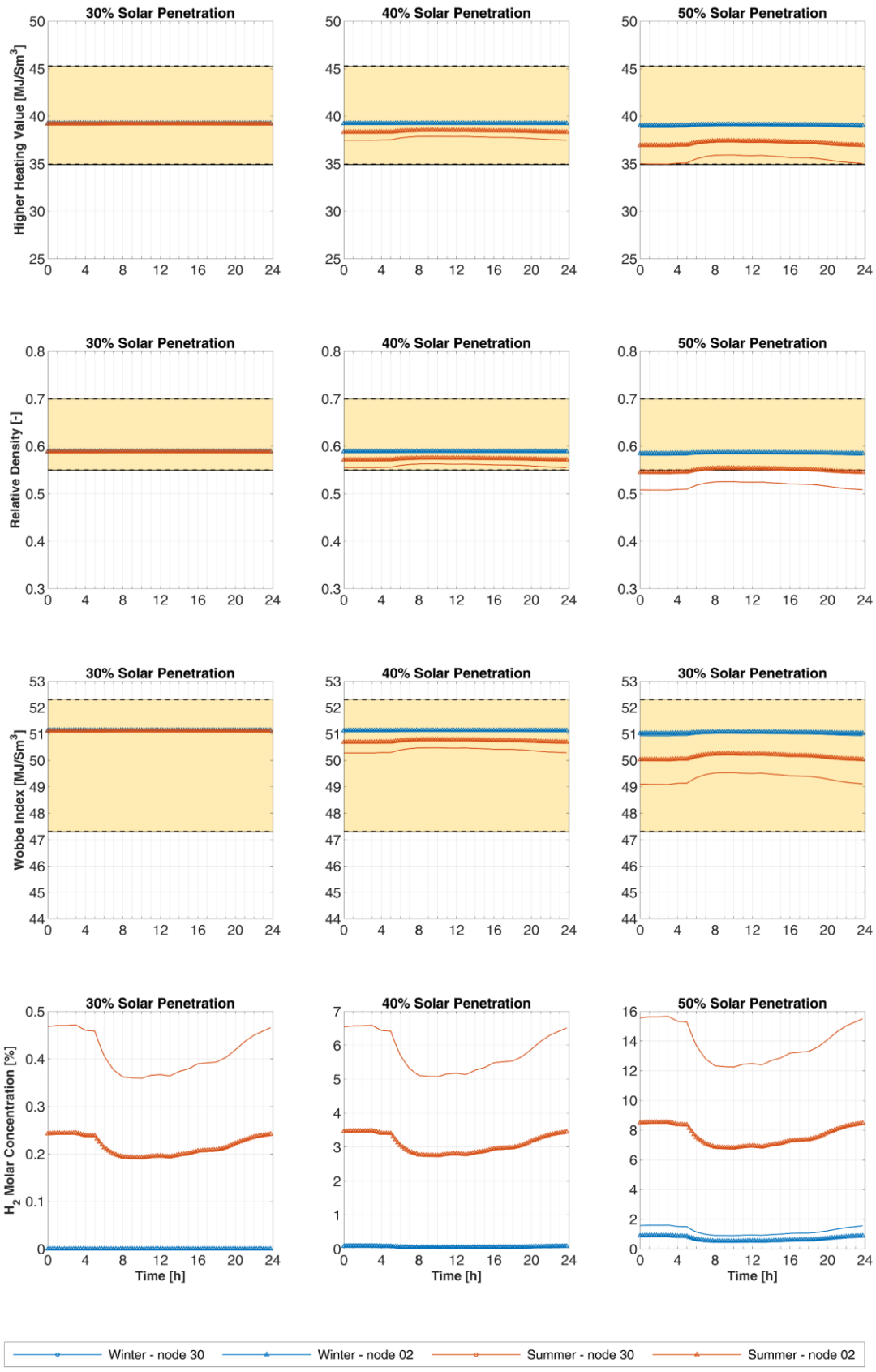

Figure 15 – Daily variation of gas quality parameters and hydrogen molar concentration for the complete set of injection scenarios, under the assumption of flat injection.

Concerning the graphs of the molar concentration of hydrogen, it is worth noting that the vertical axis scale changes through the different photovoltaic penetration cases. As the magnitude of the hydrogen injection increases (both in term of timespan and in term of peak), the hydrogen presence within natural gas increases, ranging from 7.6% to 49.3% with reference to the maximum values. These maximum values of hydrogen concentrations are obtained for the summer cases and for the case of injection at node 30.

To reduce the peaks, injecting hydrogen at an upstream node (towards the city gate) is an effective solution. As it can be seen from the picture, the maximum hydrogen concentration is reduced to 4.2%, 18.6% and 31.2% for the three stages of photovoltaic penetration when moving the injection to node 02. Moving the injection node can thus lead to halve the hydrogen percentage peak. Similar reduction results are obtained also for the winter cases and for all the cases related to the flat injections.

Flat injection patterns are more effective, by even out the peaks and spreading the injection throughout the day. The achievements in the reduction of the hydrogen percentage peaks are considerably higher: the hydrogen concentration at the maximum injection time drops to 0.4%, 5.2% and 12.5% for injection at node 30 or to 0.2%, 2.8% and 6.9% for injection at node 02 (summer case), with the hydrogen composition decrease ranging from 20 times to 4 times. However, additional installation of hydrogen storage systems would be required. The maximum storage needs in order to compensate the mismatch between solar hydrogen production and flat injection are 22.2 kg for the 30% solar penetration scenario, 271.6 kg for the 40% one and as high as 636.4 kg for the 50% case that are in line with industrial practices as reported in [77].

It is worth noting that flat injections do not mean flat concentration of hydrogen. In fact, it also depends on the withdrawal rate of natural gas from the city gate, in which a constant flux of hydrogen is to be blended, and so ultimately, it depends on the gas consumption profiles. Interestingly, in the framework of flat injections, the fluctuations of hydrogen concentration have an opposite behavior with respect to the direct injection case: hydrogen concentration is higher overnight when natural gas demand is lower. However, the variation is slow throughout the day and limited to ± 1.7%.

Concentration of hydrogen within the natural gas has a direct effect on the three gas quality parameters, as it is clear from the overall analysis of Figure 14 and Figure 15. Hydrogen blending has the effect of lowering

down both relative density and higher heating value (volume based). Consequently, the Wobbe index undergoes a reduction too. As it can be observed, relative density is the most critical parameter, as the lower limit is reached already at 30% of photovoltaic penetration, in the summer case and for direct injection at node 30. In terms of hydrogen concentration, the lower limit is reached exceeding 6.7%. Nonetheless, even at the maximum concentration for this specific case (7.6%), the Relative Density of the blend is less than 1% lower than the limit. Moving to higher photovoltaic penetration stages, the perturbation on gas quality becomes more prominent, with all the three parameters exceeding the lower limit in the summer cases, with direct injection. Relative density is almost always lower than the limits during the injection period, while higher heating value drops down to unacceptable level when the hydrogen concentration becomes higher than 15.5%. The Wobbe index instead results as the less impacted parameters, with the lower limit reached only when hydrogen concentration exceeds 29%.

Of course, the hydrogen composition limits obtained from the previous discussion depend on the quality of the natural gas at the entry point. Heavier natural gas and/or natural gas having a higher calorific value can acceptably blend more hydrogen within their stream.

From Figure 14, it is also clear how critical the direct injection of hydrogen can be in terms of gas quality acceptability and management. When performing flat injections instead (see Figure 15), all the scenarios corresponding to 30% and 40% photovoltaic penetration are acceptable. Criticalities emerge just for the summer cases at the 50% of photovoltaic penetration, both of them providing gas blends with relative density slightly lower than the lower limit, for the whole day. For injections at node 02 the relative density is –1.8% of the lower limit and for injection at node 30 it is – 8.5%.

5 Discussion

The results presented in the previous sections show that hydrogen injection practices have a minor impact on the fluid-dynamics of the network, while they may be critical with respect to natural gas quality. On a fluid-dynamic point of view, the substitution of a portion of natural gas with hydrogen implies an increase of volume flow rates through the pipeline downstream the injection because of its lower density and a lower calorific value on volume basis. This have an impact on velocity, pressure drops and pressure level at each node. For

what concerns the case study here addressed, pressure levels are negligibly affected by all the injection scenarios even though pressure drops undergoes significant relative variation with respect to the non-injection base case. Similar variation trends were obtained in [61]. This aspect may become more significant on gas networks with greater geographical extension and complexity (as it emerges from [38]), since the impact of hydrogen injection on the pressure drops is not negligible and it is strictly related to the technical features of the pipelines. The consequent variation on pressure levels may become critical in case of networks with higher pressure drops and areas with lower pressure levels already at the base case. A similar discussion may be drawn concerning the velocity. Velocity variation is higher as the percentage of hydrogen within the gas network grows. However, the velocity limits are exceeded when hydrogen concentration is lower than the maximum possible one (within the case: 50% photovoltaic penetration), and consequently, the velocity relative deviation is smaller. It is evident that the base case condition of the gas network (on a fluid-dynamic point of view), has a fundamental role in the acceptability of hydrogen blending practice. Blending smaller amount of hydrogen within a network that operates at high level of saturation of pipeline flow capacity is more critical than blending higher amount of hydrogen within a network operating with lower saturation level. This consideration applies also in case of hydrogen blending upstream the distribution gas network gate (at transmission system level).

In the context of electricity and gas sector integration, the coupling of photovoltaic energy production followed by possible hydrogen production and injection at distribution (urban) level has little been addressed. Many previous studies focused on optimal wind hydrogen integration at national infrastructure level (i.e. [53] and [55]) while the ones addressing the low-pressure local networks considered wind distributed sources [56] or unspecified hydrogen source [61] for a steady state analysis. Often the amount of acceptable hydrogen was determined *a priori* or it was not specifically addressed. The aim of this work is instead to focus on the impact of solar-hydrogen blending on a distribution infrastructure. For this reason, a detailed simulation framework of both the infrastructures has been chosen, rather than an optimization procedure.

Results showed a positive match under a fluid-dynamic point of view of the gas network, because the availability of hydrogen is higher when gas networks are less utilized resulting in a minor impact on the velocity increase.

However, the same cannot be concluded from the analysis of gas quality results. In fact, gas quality parameters are very sensitive to hydrogen concentration variation, with relative density exceeding the lower limit already when hydrogen molar concentration reaches 6.7%. Thus, under the gas quality point of view, the summer seasonality effect of hydrogen abundance and lower gas consumption brings to a negative superposition, with the gas network being challenged by the excess of renewable gas, according to the current regulatory framework. This is evident comparing the winter and the summer cases: critical concentration of hydrogen are reached already for the 30% photovoltaic penetration level at the worst summer injection case (injection at node 30), while for the winter case the critical concentration is reached at the analogous case but for the 50% photovoltaic penetration level. From an overall analysis of the results, it can be inferred that moving upstream the injection node has a slightly beneficial effect both on gas quality acceptability an on fluid-dynamic impacts. However, it is with the flat injection mode that most of the injection scenarios gain acceptability as it can be inferred from the comparison of the two acceptability matrices given in Table 4.

Table 4 – Hydrogen injection acceptability matrices: comparison between direct injection case and flat injection case, detailed for each gas parameter and the two possible injection nodes. Green: parameter within the regulatory limits; Red: parameter exceeding the regulatory limits; Limits set by [68].

Summer Case									
Direct injection profile						Flat injection profile				
Quality parameter	Photovoltaic penetration stage			Injection node		Quality parameter	Photovoltaic penetration stage			Injection node
	30%	40%	50%				30%	40%	50%	
HHV				30		HHV				30
				02						02
RD				30		RD				30
				02						02
WI				30		WI				30
				02						02

It is worth adding that flat injections have also the minimum impact on the fluid-dynamics of the gas network. Flat injections are also crucial in minimize the gas quality fluctuations. In fact, the sharp variations of gas quality corresponding to the direct injection of hydrogen (following the photovoltaic overproduction) may be even less acceptable than the exceeding of one (or more) quality parameters, in terms of grid

management and appliances functionality. On the other hand, in order to flatten the solar-hydrogen curve, the installation of daily hydrogen storages is required, adding further costs to the renewable-hydrogen local blending value-chain.

For the sake of the extension of the results to other regulatory contexts, a selection of gas quality limits from European countries [78] are provided in Figure 16, compared to the Italian ones. To be noted that Relative Density is a quality parameter which is not commonly regulated by the other countries. Concerning the lower limits of the higher heating value it is possible to note that France and UK results more susceptible to hydrogen addition, obtaining unacceptable blends already at 30% in the case of summertime direct injection at node 30. Conversely, under the Spanish regulation the case of 40% solar penetration with direct injection at node 2 may still be accepted. As for Wobbe Index, the Italian regulation appears to be the most stringent, thus considering the other European limits would allow within the acceptability ranges all the cases related to the 40% of solar penetration scenario, as well as the direct injection at node 2 of the 50% scenario.

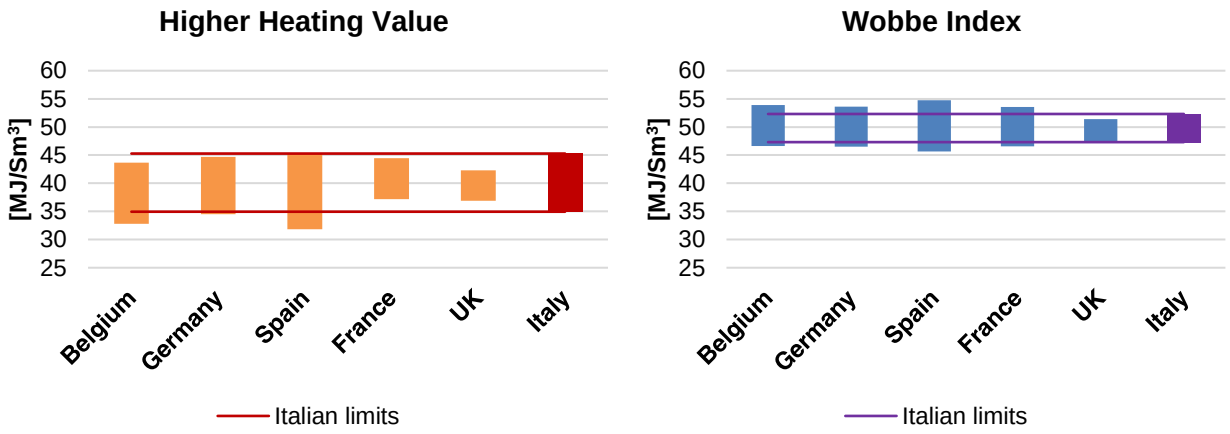

Figure 16 – Gas quality regulations ranges for higher heating value and Wobbe Index for a selection of European countries compared to the italian ones [78].

6 Conclusion

The case study presented in this paper aimed at clarifying the impacts of electricity-gas sector coupling by means of power-to-hydrogen and grid injection at urban level.

As the distributed solar generation increases, mismatches between consumption and production lead to surplus energy and reverse power flows at the HV/MV station. This power surplus gave the motivation to the sector coupling strategy by means of local hydrogen production and its injection within the gas network infrastructure of the same urban area.

Several injection cases were analysed in order to test the seasonality effect, the choice of the injection node and the injection pattern. The outcomes of the simulations showed that the injection of increasing amount of hydrogen has an impact within the gas network management, both under fluid-dynamic and gas quality point of view. On a fluid-dynamic point of view, when pipelines are operated near to the maximum flow capacity they may undergo exceeding velocity, even in case of small amount of hydrogen. This is a very case specific issue, depending on the utilization level of the addressed gas network. This outcome implies that in view of the implementation of hydrogen blending practice, the fluid-dynamic verification should be carried out case by case on the existing networks.

In the context of sector coupling, the seasonal effect insisting both on the electrical side and on the gas infrastructure has a positive superposition on fluid-dynamics, with less hydrogen injection when natural gas is at its maximum utilization rate.

On the contrary, the seasonal effect is detrimental for the gas quality. A further outcome of this study has underlined that the choice of the injection node and the hydrogen injection pattern have a prominent role in the preservation of gas quality parameters within the limits. The outcomes of the case study variants showed that the more the injection point is moved towards the root of the network (the city-gate), the more blending potential is exploited. Nevertheless, aiming at flattening the solar hydrogen production curve is the most effective way in order to limit the impact of hydrogen blending on the gas infrastructure. Thus, the installation of a hydrogen storage system is required in similar cases.

The results of the impact of increasing shares of hydrogen on the different quality parameters and the comparison among the different European gas quality regulations highlight the need for a revision of both the gas quality parameters and their limits. In addition to that, a discussion the acceptability of strong rate of variation of hydrogen within the infrastructure is desirable, as it may be an occurrence related to the direct profile injection case. In conclusion, the outcomes of this case study highlights that the integration of the

electricity and gas sectors through power-to-hydrogen and hydrogen blending at local level is not straightforward.

A proper consequential simulation algorithm for the electricity and gas sector coupling has been presented and used on a sample case study in order to simulate the impacts of solar hydrogen injection at distribution level. The algorithm can easily be applied to future works on real and more complex case studies. Several dimensions of variations may be considered ranging from different network topologies and different consumption profiles to different distributed renewable sources (wind, biomass) and different penetration strategies of both generation and consumption technologies (e.g. micro-CHP) so to contribute to gain knowledge on the actual impacts of sector coupling.

7 References

[1] The European Parliament and the Council of the European Union. Directive (EU) 2018/2001 of the European Parliament and of the Council on the promotion of the use of energy from renewable sources. Off J Eur Union 2018.

[2] Ciocia A, Boicea VA, Dematteis A, Di Leo P, Giordano F, Spertino F. PV system integration in buildings: An energy and economic case study. 2017 10th Int Symp Adv Top Electr Eng ATEE 2017 2017:786–90. https://doi.org/10.1109/ATEE.2017.7905102.

[3] Jenkins N, Ekanayake J, Strbac G. Distributed generation. Institution of Engineering and Technology; 2010.

[4] Ciocia A, Boicea VA, Chicco G, Di Leo P, Mazza A, Pons E, et al. Voltage Control in Low-Voltage Grids Using Distributed Photovoltaic Converters and Centralized Devices. IEEE Trans Ind Appl 2019;55:225–37. https://doi.org/10.1109/TIA.2018.2869104.

[5] Mazza A, Carpaneto E, Chicco G, Ciocia A. Creation of Network Case Studies With High Penetration of Distributed Energy Resources. 2018 53rd Int. Univ. Power Eng. Conf., IEEE; 2018, p. 1–6. https://doi.org/10.1109/UPEC.2018.8542025.

[6] Shahidehpour M, Wang H, Xu X, Yan Z, Zhou Q. Optimal Energy Storage Allocation for Mitigating the Unbalance in Active Distribution Network via Uncertainty Quantification. IEEE Trans Sustain Energy 2020:1.

[7] Després J. Modelling the long-term deployement of electricity storage in the global energy system. Université Grenoble Alpes, 2015.

[8] Winkler J, Breitschopf B, Ragwitz M, Mistre M, Cail S, Harmelink M. Renewable energy directive target - Study for the ITRE Commitee. 2018.

[9] Terna.it. Progetti Pilota di Accumulo 2020. https://www.terna.it/it/sistema-elettrico/innovazione-sistema/progetti-pilota-accumulo (accessed May 30, 2020).

[10] Hydrogen on the rise. Nat Energy 2016;1:16127. https://doi.org/10.1038/nenergy.2016.127.

[11] Staffell I, Scamman D, Velazquez Abad A, Balcombe P, Dodds PE, Ekins P, et al. The role of hydrogen and fuel cells in the global energy system. Energy Environ Sci 2019;12:463–91. https://doi.org/10.1039/c8ee01157e.

[12] IEA. World Energy Outlook 2019. 2019.

[13] Terna, Snam. Documento Di Descrizione Degli Scenari. 2019.

[14] Northen Gas Networks, DNV-GL. H21 project. H21 n.d. https://www.h21.green/ (accessed April 26, 2020).

[15] Snam. Snam And Hydrogen 2020. https://www.snam.it/en/hydrogen_challenge/snam_hydrogen/ (accessed May 30, 2020).

[16] Kiwa, Netbeheer Nederland. Toekomstbestendige gasdistributienetten. 2018.

[17] The heat is on. Nat Energy 2016;1:16193. https://doi.org/10.1038/nenergy.2016.193.

[18] OFGEM. Ofgem's Future Insights Series: The Decarbonisation of Heat. 2016.

[19] KPMG. 2050 Energy Scenarios: The UK Gas Networks role in a 2050 whole energy system. 2016.

[20] Unruh GC. Understanding carbon lock-in. Energy Policy 2000;28:817–30.

https://doi.org/10.1016/S0301-4215(00)00070-7.

[21] Seto KC, Davis SJ, Mitchell RB, Stokes EC, Unruh G, Ürge-Vorsatz D. Carbon Lock-In: Types, Causes, and Policy Implications. Annu Rev Environ Resour 2016;41:425–52. https://doi.org/10.1146/annurev-environ-110615-085934.

[22] ENTSOG. Ten-year network development plan 2018 executive summary. 2018.

[23] EDSO. FLEXIBILITY IN THE ENERGY TRANSITION - A Toolbox for Electricity DSOs. 2018.

[24] eurogas. FLEXIBILITY IN THE ENERGY TRANSITION - A Toolbox for Gas DSOs. 2018.

[25] Mazza A, Bompard E, Chicco G. Applications of power to gas technologies in emerging electrical systems. Renew Sustain Energy Rev 2018;92:794–806. https://doi.org/10.1016/J.RSER.2018.04.072.

[26] Ma L, Spataru C. The use of natural gas pipeline network with different energy carriers. Energy Strateg Rev 2015;8:72–81. https://doi.org/10.1016/j.esr.2015.09.002.

[27] Pellegrino S, Lanzini A, Leone P. Greening the gas network – The need for modelling the distributed injection of alternative fuels. Renew Sustain Energy Rev 2017;70:266–86. https://doi.org/10.1016/j.rser.2016.11.243.

[28] Rotunno P, Lanzini A, Leone P. Energy and economic analysis of a water scrubbing based biogas upgrading process for biomethane injection into the gas grid or use as transportation fuel. Renew Energy 2017;102:417–32. https://doi.org/10.1016/j.renene.2016.10.062.

[29] Giglio E, Lanzini A, Santarelli M, Leone P. Synthetic natural gas via integrated high-temperature electrolysis and methanation: Part II—Economic analysis. J Energy Storage 2015;2:64–79. https://doi.org/10.1016/j.est.2015.06.004.

[30] Pöyry. Fully decarbonising Europe's energy system by 2050 Decarbonising Europe's energy system. 2018.

[31] Ecofys. Gas for Climate: How gas can help to achieve the Paris Agreement target in an affordable way. 2018.

[32] Speirs J, Balcombe P, Johnson E, Martin J, Brandon N, Hawkes A. A greener gas grid: what are the options? 2017.

[33] Melaina MW, Antonia O, Penev M. Blending Hydrogen into Natural Gas Pipeline Networks : A Review of Key Issues. 2013.

[34] Dmytrakh IM, Leshchak RL, Syrotyuk AM. Effect of hydrogen concentration on strain behaviour of pipeline steel. Int J Hydrogen Energy 2015;40:4011–8. https://doi.org/10.1016/j.ijhydene.2015.01.094.

[35] Cheng L, Li L, Zhang X, Liu J, Wu K. Numerical simulation of hydrogen permeation in steels. Electrochim Acta 2018;270:77–86. https://doi.org/10.1016/j.electacta.2018.03.061.

[36] Bouledroua O, Hafsi Z, Djukic MB, Elaoud S. The synergistic effects of hydrogen embrittlement and transient gas flow conditions on integrity assessment of a precracked steel pipeline. Int J Hydrogen Energy 2020;45:18010–20. https://doi.org/10.1016/j.ijhydene.2020.04.262.

[37] Iskov H. Field test of hydrogen in the natural gas grid. 2010.

[38] Wang B, Liang Y, Zheng J, Qiu R, Yuan M, Zhang H. An MILP model for the reformation of natural gas pipeline networks with hydrogen injection. Int J Hydrogen Energy 2018;43:16141–53. https://doi.org/10.1016/j.ijhydene.2018.06.161.

[39] Altfeld K, Pinchbeck D. Admissible hydrogen concentrations in natural gas systems. Gas Energy 2013:1–12.

[40] The European Parliament and the Council of the European Union. Regulation (EU) 2016/426 of the European Parliament and of the Council on appliances burning gaseous fuels. Off J Eur Union 2016;L 81:99–145. https://doi.org/http://eur-lex.europa.eu/pri/en/oj/dat/2003/l_285/l_28520031101en00330037.pdf.

[41] UNI/EN. UNI EN 437:2019 - Test gases -Test pressures - Appliance categories 2019.

[42] Lo Basso G, Nastasi B, Astiaso Garcia D, Cumo F. How to handle the Hydrogen enriched Natural Gas blends in combustion efficiency measurement procedure of conventional and condensing boilers. Energy 2017;123:615–36. https://doi.org/10.1016/j.energy.2017.02.042.

[43] Leicher J, Nowakowski T, Giese A, Görner K. Power-to-gas and the consequences: Impact of higher hydrogen concentrations in natural gas on industrial combustion processes. Energy Procedia 2017;120:96–103. https://doi.org/10.1016/j.egypro.2017.07.157.

[44] de Vries H, Mokhov A V., Levinsky HB. The impact of natural gas/hydrogen mixtures on the performance of end-use equipment: Interchangeability analysis for domestic appliances. Appl Energy 2017;208:1007–19. https://doi.org/10.1016/J.APENERGY.2017.09.049.

[45] Directorate-General For Energy and Transport. Mandate to CEN for standardisation in the field of gas qualities 2007.

[46] UNI/EN. UNI 16726:2018 2018.

[47] Chaudry M, Jenkins N, Strbac G. Multi-time period combined gas and electricity network optimisation. Electr Power Syst Res 2008;78:1265–79. https://doi.org/10.1016/j.epsr.2007.11.002.

[48] Pambour KA, Sopgwi RT, Hodge BM, Brancucci C. The value of day-ahead coordination of power and natural gas network operations. Energies 2018;11:1–23. https://doi.org/10.3390/en11071628.

[49] Pambour KA, Bolado-Lavin R, Dijkema GPJ. An integrated transient model for simulating the operation of natural gas transport systems. J Nat Gas Sci Eng 2016;28:672–90. https://doi.org/10.1016/j.jngse.2015.11.036.

[50] Energy Exemplar. PLEXOS. Available On-Line 2020. https://energyexemplar.com/ (accessed February 6, 2020).

[51] Vaccariello E, Leone P, Canavero FG, Stievano IS. Topological modelling of gas networks for co-simulation applications in multi-energy systems. Math Comput Simul 2020. https://doi.org/10.1016/j.matcom.2019.12.018.

[52] Zeng Q, Fang J, Li J, Chen Z. Steady-state analysis of the integrated natural gas and electric power system with bi-directional energy conversion. Appl Energy 2016;184:1483–92. https://doi.org/10.1016/j.apenergy.2016.05.060.

[53] Qadrdan M, Abeysekera M, Chaudry M, Wu J, Jenkins N. Role of power-to-gas in an integrated gas and electricity system in Great Britain. Int J Hydrogen Energy 2015;40:5763–75. https://doi.org/10.1016/j.ijhydene.2015.03.004.

[54] Clegg S, Mancarella P. Integrated Modeling and Assessment of the Operational Impact of Power-to-Gas (P2G) on Electrical and Gas Transmission Networks. IEEE Trans Sustain Energy 2015;6:1234–44. https://doi.org/10.1109/TSTE.2015.2424885.

[55] Clegg S, Mancarella P. Storing renewables in the gas network: modelling of power-to-gas seasonal storage flexibility in low-carbon power systems. IET Gener Transm Distrib 2015;10:566–75. https://doi.org/10.1049/iet-gtd.2015.0439.

[56] He GX, Yan H guang, Chen L, Tao WQ. Economic dispatch analysis of regional Electricity–Gas system integrated with distributed gas injection. Energy 2020;201:117512.

https://doi.org/10.1016/j.energy.2020.117512.

[57] Guandalini G, Colbertaldo P, Campanari S. Dynamic modeling of natural gas quality within transport pipelines in presence of hydrogen injections. Appl Energy 2017;185:1712–23. https://doi.org/10.1016/J.APENERGY.2016.03.006.

[58] Chaczykowski M, Zarodkiewicz P. Simulation of natural gas quality distribution for pipeline systems. Energy 2017;134:681–98. https://doi.org/10.1016/j.energy.2017.06.020.

[59] Cavana M, Lanzini A, Leone P. Hydrogen blending into the gas distribution grid: the case study of a small municipality 2018:11–9.

[60] ISO. ISO 12213-3:2006 - Natural Gas: Calculation of compression factor - Part 3: Calculation using physical properties 2006.

[61] Abeysekera M, Wu J, Jenkins N, Rees M. Steady state analysis of gas networks with distributed injection of alternative gas. Appl Energy 2015;164:991–1002. https://doi.org/10.1016/j.apenergy.2015.05.099.

[62] Shirmohammadi D, Hong HW, Semlyen A, Luo GX. A compensation-based power flow method for weakly meshed distribution and transmission networks. IEEE Trans Power Syst 1988;3:753–62. https://doi.org/10.1109/59.192932.

[63] Cavana M, Leone P. Biogas blending into the gas grid of a small municipality for the decarbonization of the heating sector. Biomass and Bioenergy 2019;127. https://doi.org/10.1016/j.biombioe.2019.105295.

[64] Colebrook CF, White CM, Taylor GI. Experiments with fluid friction in roughened pipes. Proc R Soc London Ser A - Math Phys Sci 1937;161:367–81. https://doi.org/10.1098/rspa.1937.0150.

[65] Poling BE, Prausnitz JM. The Properties of Gases and Liquids. 5th ed. 2001.

[66] JRC. PV-GIS n.d. http://re.jrc.ec.europa.eu/pvgis/.

[67] Marcogaz, eurogas, GERG. Gas Bridges : the natural gas network as key partner of the energy transition. 2017.

[68] Italian Ministry of the Interior. D.M. 18/05/2018 - Regola tecnica sulle caratteristiche chimico fisiche e sulla presenza di altri componenti nel gas combustibile 2018.

[69] Pilo F, Pisano G, Scalari S, Dal Canto D, Testa A, Langella R, et al. ATLANTIDE - Digital archive of the Italian electric distribution reference networks. CIRED 2012 Work. Integr. Renewables into Distrib. Grid, IET; 2012, p. 165–165. https://doi.org/10.1049/cp.2012.0783.

[70] Mazza A, Cavana M, Mercado Medina EL, Chicco G, Leone P. Creation of Representative Gas Distribution Networks for Multi-vector Energy System Studies. 2019 IEEE Int Conf Environ Electr Eng 2019 IEEE Ind Commer Power Syst Eur (EEEIC / I&CPS Eur 2019:1–6. https://doi.org/10.1109/EEEIC.2019.8783701.

[71] Italian Ministry of the Interior. D.M. 24-11-1984 - Norme di sicurezza antincendio per il trasporto, la distribuzione, l'accumulo e l'utilizzazione del gas naturale con densità non superiore a 0,8 1984;8.

[72] Sabatini F. Criteri di progettazione di reti ed impianti per la distribuzione del gas naturale. Edizioni Consiag; 1990.

[73] Tarenzi V, Cerè A, Caimo F. Calcolo del regime stazionario di una rete di trasporto e di distribuzione del gas (bassa, media ed alta pressione). open source; 2015.

[74] Ferrero D, Gamba M, Lanzini A, Santarelli M. Power-to-Gas Hydrogen: Techno-economic Assessment of Processes towards a Multi-purpose Energy Carrier. Energy Procedia, vol. 101, 2016, p. 50–7.

https://doi.org/10.1016/j.egypro.2016.11.007.

[75] Schmidt O, Gambhir A, Staffell I, Hawkes A, Nelson J, Few S. Future cost and performance of water electrolysis: An expert elicitation study. Int J Hydrogen Energy 2017;42:30470–92. https://doi.org/10.1016/j.ijhydene.2017.10.045.

[76] ARERA. 229/2012/R/GAS - Testo integrato delle disposizioni dell'Autorità per l'energia elettrica e il gas in ordine alla regolazione delle partite fisiche ed economiche del servizio di bilanciamento del gas naturale (Settlement) 2012:1–17.

[77] Simonis B, Newborough M. Sizing and operating power-to-gas systems to absorb excess renewable electricity. Int J Hydrogen Energy 2017;42:21635–47. https://doi.org/10.1016/j.ijhydene.2017.07.121.

[78] European Union. Types of gas and the corresponding supply pressures according to Article 4(1) of Regulation (EU) 2016/426 of the European Parliament and of the Council on appliances burning gaseous fuels and repealing Directive 2009/142/EC 2018:1–28.